Geochimica et Cosmochimica Acta 345 (2023) 75–89

Contents lists available at ScienceDirect

Geochimica et Cosmochimica Acta

journal homepage: www.elsevier.com/locate/gca

Assessing the reliability of modern marine stromatolites as archives for the uranium isotope paleoredox proxy

Ashley N. Martin [a,*], Monika Markowska [b], Allan R. Chivas [c,d], Stefan Weyer [a]

[a] Institut für Mineralogie, Leibniz Universität Hannover, Callinstraße 3, Hannover, Germany
[b] Max Planck Institute for Chemistry, Climate Geochemistry Department, Mainz, Germany
[c] GeoQuEST Research Centre, School of Earth, Atmospheric and Life Sciences, University of Wollongong, NSW 2522, Australia
[d] Department of Earth Sciences and Sprigg Geobiology Centre, University of Adelaide, SA 5005, Australia

ARTICLE INFO

Article history:
Received 16 May 2022
Accepted 13 January 2023
Available online 20 January 2023
Associate editor: Claudine Stirling

Keywords:
Stromatolite
Uranium isotopes
Redox
Seawater

ABSTRACT

Uranium isotopes ($^{238}U/^{235}U$) are commonly utilised in marine carbonates to reconstruct the redox evolution of ancient oceans and the atmosphere. However, questions remain concerning U isotope fractionation during carbonate precipitation and/or early sedimentary diagenesis. Moreover, the stromatolitic nature of many Precambrian limestones and dolostones brings further questions about U isotope fractionation during stromatolite formation due to microbial activity. Thus, it is unclear whether stromatolites are reliable archives for the U isotope composition of seawater. Here we measure the $^{238}U/^{235}U$ ratio of modern stromatolites from the hypersaline Shark Bay, Western Australia, a key study area that represents the largest modern example of stromatolite growth globally. A component-specific approach was utilised to analyse the uppermost crusts of modern stromatolites, older material from the deeper stromatolite laminae and the substrate upon which the stromatolites are forming. Our interpretations of $\delta^{238}U$ data are aided by $\delta^{234}U$, $\delta^{18}O$, $\delta^{13}C$ and trace element measurements, including some mineralogy and total organic carbon determinations for selected samples.

Modern aragonitic crusts of stromatolites from the subtidal and intertidal zones around Shark Bay exhibited a narrow range of $\delta^{238}U$ (−0.30 to −0.33‰), corresponding to a small offset of ca. +0.07‰ from seawater. This range of $\delta^{238}U$ values overlaps with that of other primary carbonate precipitates in shallow marine environments such as corals but with a slightly higher mean $\delta^{238}U$. We investigated if this offset may be associated with the coprecipitation of U with aragonite from hypersaline seawater in Shark Bay, which has a higher proportion of dissolved U present as $Ca_2UO_2(CO_3)_3$ compared to open seawater. However, this measured offset is much smaller than that predicted using a speciation-dependent isotope fractionation model. Sub-recent material in the deeper stromatolite laminae exhibited higher and more variable $\delta^{238}U$ (up to −0.15‰) compared to the modern aragonitic crusts of stromatolites. The strong inverse correlation between $\delta^{238}U$ and the total organic carbon content ($r = -0.83$) and positive correlation with Mn concentrations ($r = 0.91$) suggest that ^{238}U was preferentially reduced in the deeper laminae in association with organic carbon remineralisation under reducing conditions. The average $\delta^{238}U$ offset of sub-recent stromatolite laminae from modern seawater was +0.13 ± 0.11‰ (1 s.d.), which is slightly lower than, but within uncertainty of, the offset measured for bulk carbonates from the Bahamas (+0.27 ± 0.14‰; 1 s.d.). These results demonstrate that stromatolites are valuable archives of global seawater $\delta^{238}U$, even in hypersaline restricted basins such as Shark Bay, but an offset to account for syndepositional diagenesis is likely required to accurately reconstruct seawater $\delta^{238}U$ using ancient stromatolites.

1. Introduction

The application of novel metal isotope redox systems such as uranium (U) isotopes to marine carbonates has revealed new insights into marine oxygenation and deoxygenation events in Earth's history (Brennecka et al., 2011; Dahl et al., 2014; Elrick et al., 2017; Jost et al., 2017; Lau et al., 2017; Clarkson et al., 2018; Tissot et al., 2018; Wang et al., 2018; Zhang et al., 2018; Gilleaudeau et al., 2019; Tostevin et al., 2019; Brüske et al., 2020a; Chen et al., 2021; Clarkson et al., 2021) but such interpretations require careful considerations due to the potential alter-

* Corresponding author.
E-mail address: a.martin@mineralogie.uni-hannover.de (A.N. Martin).

https://doi.org/10.1016/j.gca.2023.01.011
0016-7037/

ation of U isotope signatures in carbonates during sedimentary diagenesis (Romaniello et al., 2013; Hood et al., 2016; Chen et al., 2018a; Tissot et al., 2018; del Rey et al., 2020; Zhang et al., 2020). An as yet unexplored avenue is potential U isotope fractionation effects associated with microbially influenced (or mediated) carbonate precipitation, which should be assessed to reliably reconstruct oceanic redox conditions in deep time using microbial carbonate archives.

Precambrian marine carbonates commonly contain stromatolitic units, with a mean prevalence of ~40 to almost 100% throughout the Archean and Proterozoic (Peters et al., 2017). Stromatolites are a subset of microbialites, i.e., lithified organosedimentary structures that form in shallow water by the trapping and binding of sediment grains, and/or the precipitation of calcium carbonate by microbial communities, where laminated and unlaminated accumulations are termed stromatolites and thrombolites, respectively (Riding, 2011). Stromatolites were likely present from at least 3.5 Ga (Allwood et al., 2006) or as early as 3.7 Ga (Nutman et al., 2016), one billion years before the Great Oxidation Event at ~2.4 to 2.3 Ga when Earth's atmosphere–ocean system shifted from generally reducing to oxidising conditions (Farquhar et al., 2000; Holland, 2002; Bekker et al., 2004). The abundance of stromatolites in the geological record began to decrease around 1 Ga, and then abruptly declined following the Cambrian explosion at around 540 Ma, possibly due to the rise of metazoans (Walter and Heys, 1985), or changes in seawater chemistry (Grotzinger, 1990; Peters et al., 2017). It is commonly thought that modern stromatolites only occur in extreme, low nutrient environments where most other life forms cannot survive, e.g., Shark Bay, Western Australia (hypersaline marine embayment), Yellowstone National Park, U.S. (hot springs), etc. However, modern stromatolites also occur in habitable environments such as in open-marine (normal salinity) conditions in the Bahamas (Dravis, 1982) and the freshwater Pavilion Lake, Canada (Brady et al., 2010). In fact, the common feature shared by these localities is unusually high alkalinity and elevated concentrations of carbonate-forming cations (Ca and Mg). This is consistent with the seawater chemistry hypothesis proposed by Grotzinger (1990) and Peters et al. (2017) for the decline of stromatolite abundance in the geological record. Moreover, this suggests that the aqueous geochemistry in each of these modern settings where modern stromatolites can proliferate likely shares at least some commonalities with ancient environments that hosted stromatolites. Thus, despite the generally reducing conditions in some ancient settings, e.g., during the Archean (Farquhar et al., 2000; Holland, 2002; Bekker et al., 2004), modern stromatolites are useful for improving our understanding of how metal redox proxies, such as U isotopes, are archived in stromatolites, under the end-member scenario of a fully oxygenated atmosphere–ocean system.

Uranium is a redox-sensitive metal that is present at Earth's surface as the insoluble U(IV) and more soluble U(VI). In oxic near-surface environments, U(VI) forms stable uranyl carbonate complexes with Ca and Mg, e.g., Ca-UO_2-CO_3 (Endrizzi et al., 2016; Chen, 2020), leading to a relatively high concentration (3 ng/g) and long residence time (~0.5 Ma) in modern oceans (Andersen et al., 2017). Under reducing conditions, U(IV) is insoluble and enriched in anoxic sedimentary deposits. In the last decade, variations in the ratio of the two primordial U isotopes (^{238}U and ^{235}U) have been detected in sediments, accessory minerals and low temperature U deposits (Stirling et al., 2007; Weyer et al., 2008; Andersen et al., 2017). According to *ab initio* modelling, equilibrium U isotopic fractionation is dominated by the nuclear field shift effect, resulting in U isotopic fractionation occurring in the opposite direction to mass-dependent isotope fractionation (Bigeleisen, 1996; Schauble, 2007; Abe et al., 2008; Fujii et al., 2009). Thus, reduced U is enriched in ^{238}U, consistent with higher $\delta^{238}U$ values for modern anoxic sediments (Weyer et al., 2008; Andersen et al., 2014; Brüske et al., 2020b), and low-temperature U ore deposits (Murphy et al., 2014). In contrast, U adsorption onto iron and manganese (oxy)hydroxides results in a slight enrichment of ^{235}U and lower $\delta^{238}U$ values (Weyer et al., 2008; Brennecka et al., 2011; Goto et al., 2014). In addition to carbonate records, shales and iron formations are typically utilised as archives for paleo-seawater, particularly in Precambrian studies (e.g., Wang et al., 2018; Brüske et al., 2020a; Chen et al., 2021).

Modern primary carbonate precipitates from shallow-marine environments such as corals, molluscs, green algae, red algae and echinoderms generally record seawater-like $\delta^{238}U$ values (Stirling et al., 2007; Weyer et al., 2008; Romaniello et al., 2013; Chen et al., 2018b; Tissot et al., 2018; Livermore et al., 2020; Kipp et al., 2022a). Interestingly, the magnitude of isotope fractionation in these carbonates (0.00–0.09‰) is less than that predicted by abiotic $CaCO_3$ coprecipitation experiments (0.11 ± 0.02‰) (Chen et al., 2016), possibly facilitating distinct mechanisms of U isotope fractionation during stromatolite formation due to the unusual seawater chemistry (Chen et al., 2017). A much larger offset from seawater of +0.27 ± 0.14‰ was measured in a shallow core in the Bahamas, which was attributed to authigenic U accumulation into carbonate components under reducing conditions during early diagenesis (Romaniello et al., 2013; Chen et al., 2018a). Late-stage diagenesis may also be important as demonstrated by the different carbonate components of a Cryogenian limestone exhibiting variable $\delta^{238}U$ from −0.7 to −0.1‰ (Hood et al., 2016). As stromatolites may also accrete via binding and trapping detrital sediment, care must be taken to selectively dissolve the carbonate fraction to accurately reconstruct past changes in the U isotope composition of seawater (Plater et al., 1992; Clarkson et al., 2020).

In this study, we investigate U isotope fractionation during formation and early diagenesis of modern stromatolites in order to assess their suitability as archives for the U isotope composition of Precambrian seawater. As a case study, we analysed stromatolites from Hamelin Pool in Shark Bay World Heritage Area, Western Australia – the largest occurrence of modern stromatolites globally (Jahnert and Collins, 2012; Suosaari et al., 2016). In addition, we analyse the $\delta^{13}C$, $\delta^{18}O$ and trace element composition of modern stromatolites, the water isotopes ($\delta^{2}H$ and $\delta^{18}O$) of groundwater and seawater samples, and the mineralogical composition of stromatolite laminae. Leaching experiments were also conducted with stromatolite material to evaluate the ideal protocol for accurately reconstructing seawater $\delta^{238}U$. The modern stromatolites at Shark Bay are excellent analogues for Precambrian stromatolites because: (1) they host many microbial communities that have retained their anaerobic capabilities associated with anoxic conditions (Wong et al., 2015); (2) the lithification of modern microbial mats at Shark Bay occurs by microcrystalline carbonate (micrite) precipitation as both a framework and cement, which is a key biosignature of microbial activity (Reid et al., 2003; Dupraz et al., 2009; Suosaari et al., 2016); and (3) many important examples of Precambrian stromatolites likely formed in restricted marine settings, e.g., those from the 2.7 Ga Tumbiana Formation (Bolhar et al., 2002), the 3.0 Ga Pongola Supergroup (Bolhar et al., 2015) and the 3.4 Ga Strelley Pool Chert (Allwood et al., 2006).

2. Study area: Hamelin Pool, Shark Bay, Western Australia

Shark Bay World Heritage Area is a large coastal embayment in Western Australia with a large salinity gradient due to the various degrees of restriction with the open ocean (Fig. 1), most notably due to the Faure Sill, a sandy embankment covered by seagrass. Microbial structures mainly occur in Hamelin Pool (Fig. 1) and microbialite growth covers almost the entire coastline (Jahnert

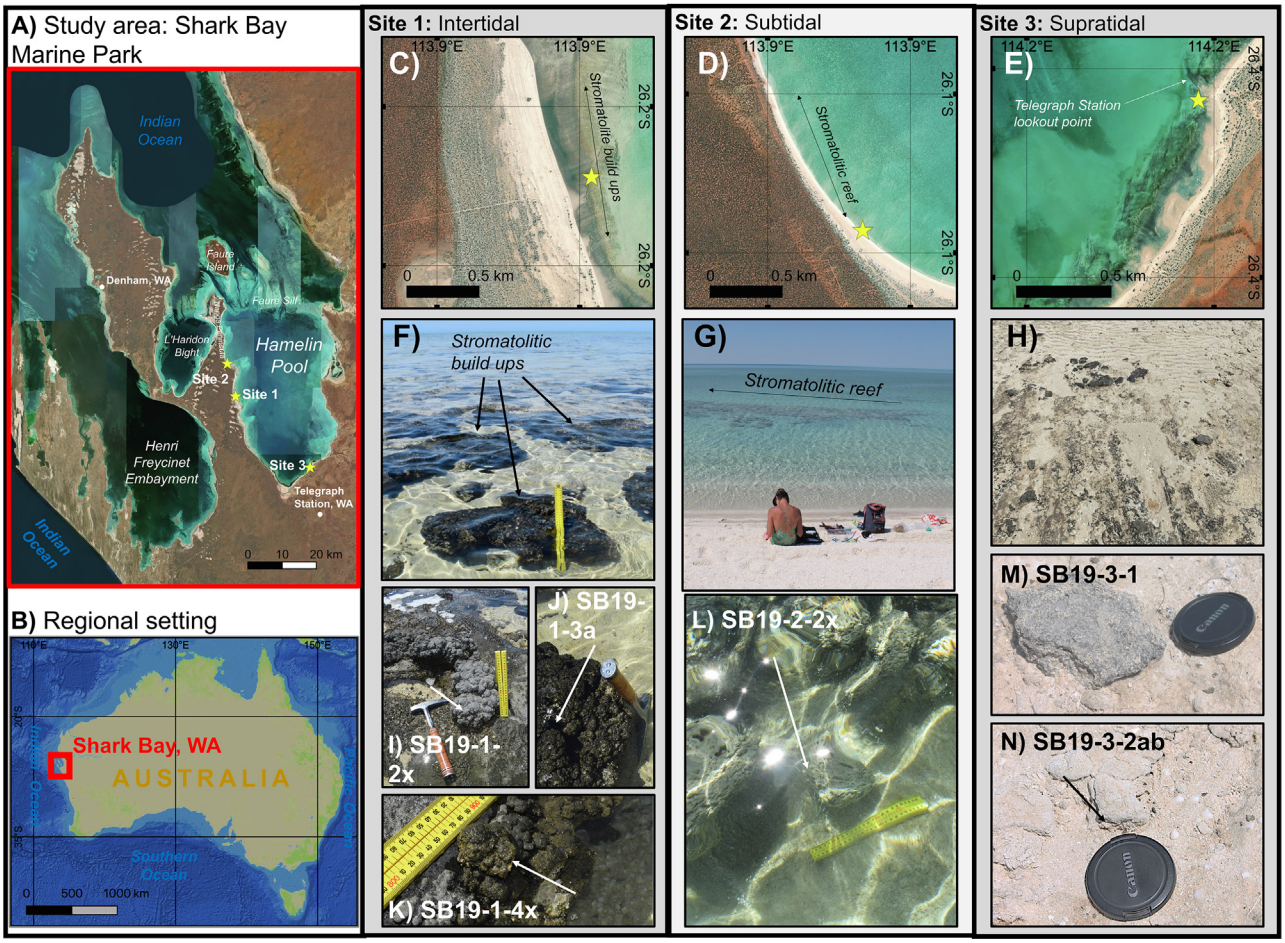

Fig. 1. Maps showing the location of the study area in (A) Shark Bay Marine Park, and (B) Australia. Satellite imagery (C–E; yellow stars show exact sampling location) and ground images (F–H) of the three sampling locations (Sites 1–3), respectively. Images of sampling locations of (I) SB19-1-2x, (J) SB19-1-3a, (K) SB19-1-4x, (L) SB19-2-2x, (M) SB19-3-1, and (N) SB19-3-2ab. Geological hammer, ruler (cm scale) and camera lens cover for scale. The shells in (N) are the bivalve *Fragum erugatum*. (For interpretation of the references to colour in this figure legend, the reader is referred to the web version of this article.)

and Collins, 2012; Suosaari et al., 2016; Morris et al., 2020). Hamelin Pool is the most restricted embayment in Shark Bay, covering an area of ~1,400 km^2 and is hypersaline (average: 66 PSU; Suosaari et al., 2016) with a maximum depth of 11 m. The presence of actively growing stromatolites in Hamelin Pool was first noted in the 1960s and is the largest modern example of modern stromatolite growth by areal extent (Logan, 1961; Playford and Cockbain, 1976). Stromatolite formation began in Shark Bay at around 2 ka BP, corresponding to growth rates ranging from <1 to 50 cm/ka (Chivas et al., 1990; Jahnert and Collins, 2012).

Extensive mapping campaigns on various scales have revealed that diverse stromatolite morphologies and microbial communities are present across Hamelin Pool as a function of shelf bathymetry and water energy (Logan, 1961; Jahnert and Collins, 2012; Suosaari et al., 2016; Morris et al., 2020). In addition to discrete stromatolite build-ups, another important microbial structure at Shark Bay is 'microbial pavement', which is a flat, light grey deposit with a tabular or blocky surface morphology that covers 227 km^2 of the subtidal surface in Hamelin Pool (Jahnert and Collins, 2012); due a fall in sea-level since the mid-Holocene, large deposits of microbial pavement are now exposed in the supratidal zone around Shark Bay.

The principal microbial structures at Shark Bay according to their surficial microbial mat type are: (1) smooth (e.g., Fig. 2E and F), (2) 'pustular' (uneven, blistered surfaces; e.g. Fig. 2B), (3) 'colloform' (hemispherical globular morphology; e.g. Fig. 2C), and (4) 'cerebroid' (irregular fenestral fabric with voids; Fig. 2D; Logan, 1961; Jahnert and Collins, 2012; Wong et al., 2015; Suosaari et al., 2016). However, care should be taken when classifying stromatolites based on their mat type as lithified build-ups may have been formed by various microbial communities over time and have distinct morphologies and internal fabrics (Suosaari et al., 2016). This problem may be overcome by sampling the modern aragonitic crusts of stromatolites, which represents the uppermost few centimetres of a stromatolite surface that contains the active microbial mat and is in contact with the external air or water boundary. This is distinct from 'older, deeper stromatolite laminae' that are more lithified and do not contain an active microbial mat. The 'stromatolite substrate', i.e., the surface upon which the stromatolites are forming, can typically be visually distinguished from stromatolite laminae at Shark Bay due to their reduced porosity, which is associated with the seafloor carbonate lithification processes and are commonly carbonate hardgrounds (Chivas et al., 1990).

3. Field sampling

Stromatolites were sampled from Hamelin Pool in the Shark Bay World Heritage Area, Western Australia (hereafter 'Shark Bay') in two separate field campaigns. The modern aragonitic crusts of stromatolites were collected from three field sites around Shark Bay in October 2019. Each site was classified according to the tidal zone:

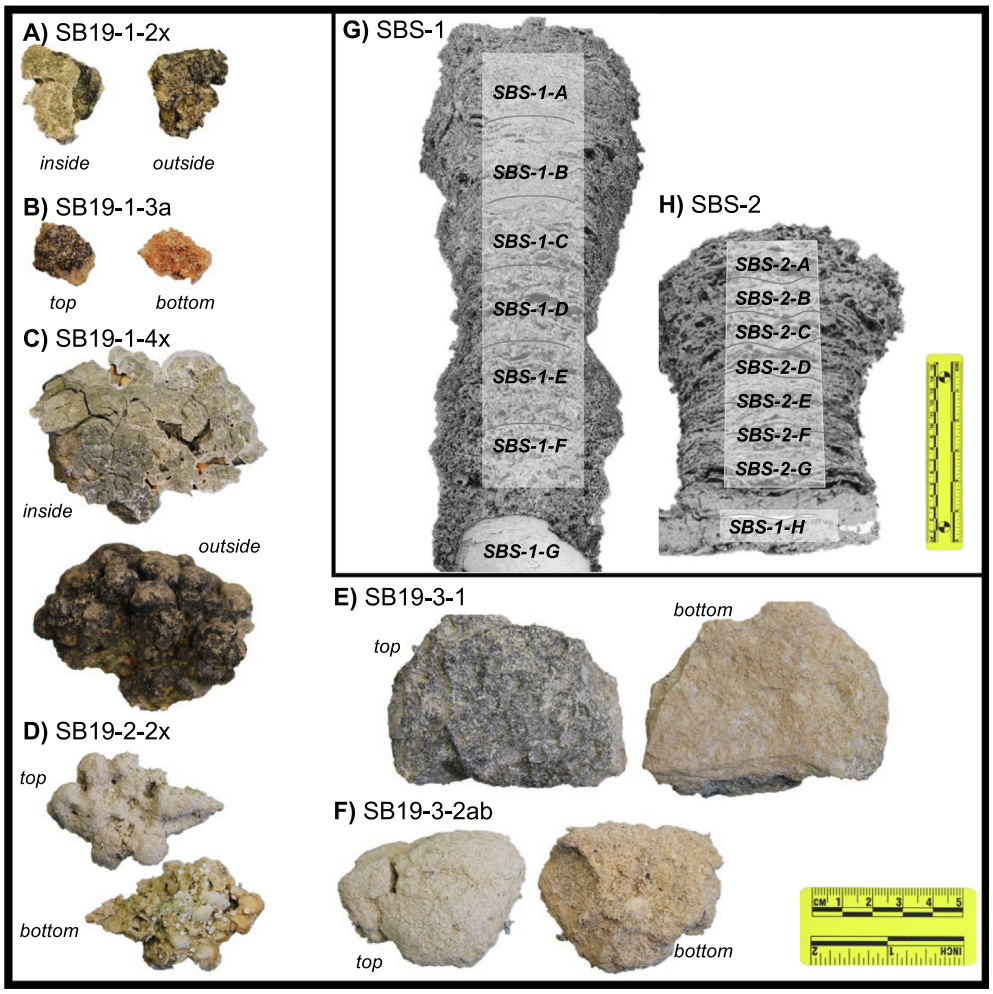

Fig. 2. Images of samples (A) SB19-1-2x, (B) SB19-1-3a, (C) SB19-1-4x, (D) SB19-2-2x, (E) SB19-3-1, (F) SB19-3-2ab, (G) SBS-1 and (H) SBS-2. The 5-cm scale ruler applies to images A-F whereas a 15-cm scale ruler is shown in (G) and (H).

(1) intertidal zone (stromatolite surfaces exposed at low tide), (2) subtidal zone (stromatolite surfaces remain covered at low tide), and (3) supratidal zone (entire stromatolite located above the average high-water line; Fig. 1; sample locations given in Table 1). The intertidal crusts were collected from the surfaces of three different stromatolites with colloform (SB19-1-2x and SB19-1-4x) and pustular mat types (SB19-1-3a; Fig. 2). The subtidal sample SB19-2-2x was sampled from a stromatolite with a cerebroid mat type. Smooth mats were sampled from the supratidal zone (SB19-3-1 and SB19-3-2ab) and are interpreted as microbial pavement (see Section 2; Jahnert and Collins, 2012). The modern aragonitic crusts of stromatolites were air dried in the field prior to shipping.

Stromatolites SBS-1 and SBS-2 (Fig. 2G and H) are discrete stromatolite build-ups that were originally sampled by Chivas et al. (1990) from the subtidal and intertidal zones at Playford's Site (2.8 km south of Flagpole Landing that corresponds to Site 3 in Fig. 1), respectively, and then stored at the National Palaeontological Collection, Geoscience Australia, in Canberra. The average growth rates of SBS-1 and SBS-2 were 29 cm/ka and 19 cm/ka, respectively (Chivas et al., 1990) and both stromatolites comprise predominantly (>50%) sand-size carbonate grains that are fused together by a micritic matrix. Thus, they can be considered as *calcarenite stromatolites*, which are commonly found forming in both Shark Bay and the Bahamas (Reid et al., 2003). The substrate of SBS-2 is a hardground with a similar aragonitic mineralogy and has a similar radiocarbon age to the older stromatolite laminae, suggesting that stromatolitic development commenced shortly after lithification of marine sediments in Shark Bay. In contrast, the substrate at the base of SBS-1 (SBS-1G; Fig. 2) has a much older radiocarbon age (>15 ka BP) than the stromatolite laminae and is composed of calcite. This material likely represents a fragment of calcrete from the late Pleistocene Bibra Limestone or was lithified some time before 15 ka BP (Chivas et al., 1990).

During the 2019 sampling campaign, two seawater samples were collected from two locations in Shark Bay (Site 1 and Site 2), in addition to a shallow groundwater bore sample (SB19-3). Before water samples were taken, temperature, pH, electrical conductivity, dissolved oxygen and oxidation reduction potential (ORP) were measured using a HI98194 multi-meter instrument. The groundwater well was purged until stabilisation of in-field parameters before groundwater samples were collected. On the same day of sampling, all water samples were filtered at 0.45 μm and total alkalinity concentrations were determined by a double endpoint titration method using a Hach digital titrator. Water samples for cation analysis and U isotope measurements were acidified to 1% v/v HNO_3 for laboratory analysis.

4. Analytical methods

In the laboratory, the samples from the 2019 field campaign were further dried in an oven overnight at 80 °C, and then powdered and homogenised in an agate mortar and pestle prior to geo-

Table 1
Hydrochemical parameters, major cation and anions, and U concentrations for water samples.

Sample ID	Site	Type	Lat.	Long.	pH	ORP	EC	Salinity	Temp.	TA	Na	Ca	Mg	Cl	$\delta^{18}O$	$\delta^{2}H$	U	$\delta^{234}U$	$\delta^{238}U$
						mV	*mS/cm*	*PSU*	°C	*mg/L*	*mg/l*	*mg/l*	*mg/l*	*g/l*	‰	‰	*µg/l*	‰	‰
SB19-1 (site 1)	Hamelin Pool	sw	−26.21	113.94	8.08	202	91.8	65.6	25.4	132	18,100	604	2,029	36.4	3.8	24.1	10.9	+146.8 ± 1.4	−0.36 ± 0.02
SB19-2 (site 2)	Hamelin Pool	sw	−26.13	113.92	8.09	199	84.7	59.8	24.5	130	15,950	570	1,898	34.3	4.3	26.4	11.1	+143.5 ± 1.0	−0.37 ± 0.02
SB19-3	S-Shed bore	gw	−26.10	113.65	7.31	93	6.6	3.6	29.7	214	1,460	102	121	2.1	−5.3	−37.9	6.2	+732.8 ± 0.8	−0.18 ± 0.03

Where sw: seawater, gw: groundwater, ORP: Oxidation-reduction potential, EC: Electrical conductivity and TA: Total alkalinity.

chemical analyses. The outer areas of stromatolites SBS-1 and SBS-2 were cut and originally embedded in gypseous plaster, which was avoided during the sampling of material from the inner areas of SBS-1 and SBS-2. Nevertheless, a piece of the plaster was also sampled for ICP-MS measurements to assess the potential contribution of U. Around 1–2 g of material from the inner areas of SBS-1 and SBS-2 were sampled at approximately 7 and 3 cm intervals, respectively, including the hard calcitic substrate at the base of SBS-1 (SBS-1G; Fig. 2). Similar to the modern stromatolite material, samples from SBS-1 and SBS-2 were further dried in an oven overnight at 80 °C and then powdered in an agate mortar and pestle.

4.1. Hydrochemical analyses

The major cation and anion concentrations of water samples were analysed using ion chromatography compact IC Flex and Compact IC Plus from Metrohm at the University of Tübingen. The uncertainty for these analyses was less than ±5% for all elements. The stable isotope composition ($\delta^{18}O$ and $\delta^{2}H$) of water samples (0.4–0.5 µl) were analysed at the Max Planck Institute for Chemistry (MPIC) Mainz on a Picarro L2140-i cavity ring-down spectrometer following the 'wet background' configuration outlined in de Graaf et al. (2021). Samples were calibrated using Vienna Standard Mean Ocean Water (VSMOW) and three in-house standards with $\delta^{18}O$ isotope values of –8.78, 6.96 and 1.12‰, respectively, and $\delta^{2}H$ values of −63.3, 45.81 and 3.29‰, respectively, referenced to the international VSMOW-SLAP scale. The overall precision on these analyses was less than ±0.1‰ for $\delta^{18}O$ and 0.5‰ for $\delta^{2}H$.

4.2. Stable isotope analyses of carbonates

The stable isotope composition ($\delta^{18}O$ and $\delta^{13}C$) of stromatolite powders was analysed at the MPIC Mainz on a Thermo Delta V mass spectrometer equipped with a Gasbench preparation device. Approximately 20 to 50 µg of $CaCO_3$ powder was acidified in He-filled 12 mL exetainer vials with high purity (>99%) H_3PO_4 at 70 °C. A total of 20 replicates for two in-house $CaCO_3$ standards were analysed in each run of 55 samples and reported relative to the Vienna Pee Dee Belemnite (VPDB) standard. The overall precision on these analyses was less than ±0.1‰ for both $\delta^{18}O$ and $\delta^{13}C$.

4.3. Leaching experiments

Leaching experiments were conducted on a stromatolite powder (SB19-2-2x) before commencing trace element and U isotope analyses of the other stromatolite powders to determine the optimum acid leaching procedure. The range of weak and strong acids is given in Table 2 and is similar to those tested by Clarkson et al. (2020) on pelagic carbonates. Approximately ~200 mg Shark Bay stromatolite powder was leached using 5 mL of acid for either 1 or 24 h, at room temperature and mechanically agitated. The samples were centrifuged and the solutions were retained for analyses. Results from these experiments showed that leaching using 0.2 M acetic acid (AcOH) for 24 h was optimum (see discussion in Section 6.1 for more details).

4.4. Trace element and uranium isotope analyses of stromatolites

Approximately ~200–500 mg of stromatolite powder was weighed into 15 mL polypropylene centrifuge tubes and leached with 10 mL 0.2 M AcOH at room temperature for 24 h. The samples were centrifuged and the solutions were retained for analyses. A 0.1 mL aliquot of this solution was sampled and diluted for ICP-MS concentration measurements.

Table 2
Experimental conditions for leaching experiments on a Shark Bay stromatolite powder (SB19-2-2x) including trace element and U isotope data for the leachate fraction.

Exp.	Acid	t	Mass loss	pH start	pH end	Al	Mn	Fe	U	Th/U	$\delta^{234}U$		2 s.e.	$\delta^{238}U$		2 s.e.
		h	*wt.%*	–	–	*μg/g*	*μg/g*	*μg/g*	*μg/g*	*wt./wt.*	*‰*			*‰*		
1	0.2 M AcOH	1	53	2.8	5.8	17	3	7	0.62	0.04	148.1	±	0.1	−0.31	±	0.03
2	1 M NaAcOH	1	64	5.0	5.6	14	1	6	0.53	1.36	149.3	±	0.3	−0.31	±	0.04
3	0.5 M HCl	1	88	0.5	1.2	43	3	32	0.99	0.07	149.1	±	0.3	−0.33	±	0.01
4	3 M HCl	1	91	0.1	0.1	50	3	61	1.07	0.09	149.3	±	0.1	−0.33	±	0.01
5	3 M HNO_3	1	90	0.1	0.1	52	3	44	1.13	0.07	149.0	±	0.2	−0.33	±	0.01
6	0.2 M AcOH	24	64	2.8	5.9	13	3	4	0.85	0.03	149.7	±	0.2	−0.31	±	0.01
7	1 M NaAcOH	24	79	5.0	5.8	18	1	7	0.68	1.33	150.6	±	0.1	−0.32	±	0.02
8	0.5 M HCl	24	88	0.5	1.4	65	3	56	1.14	0.08	150.6	±	0.2	−0.36	±	0.01
9	3 M HCl	24	91	0.1	0.1	72	3	70	1.24	0.08	149.2	±	0.3	−0.31	±	0.01
10	3 M HNO_3	24	90	0.1	0.1	66	2	62	1.18	0.07	149.3	±	0.0	−0.35	±	0.01

t is time, in hours.

The remaining leachate solutions were evaporated and formed a white precipitate and 0.2 mL conc. HNO_3 and 0.6 mL conc. HCl (Aqua regia) were added to oxidise the organic compounds present prior to column chromatography. The samples were then evaporated at 80 °C to incipient dryness and redissolved in 3–5 mL 3 M HNO_3. The measured U concentration was used to optimise the addition of IRMM-3636a U double spike (Richter et al., 2008) to the samples, targeting a $^{236}U/^{235}U$ of ~3 and a molar U sample-spike ratio of ~20–25. Column chromatography to separate U from the sample matrix was conducted according to Weyer et al. (2008) using the Eichrom UTEVA resin and 150 to 300 ng U was typically loaded. Following column chromatography, 0.1 mL HNO_3 (65%) and 0.1 mL H_2O_2 (30%) were added and evaporated at 80 °C to incipient dryness. The residue was then redissolved in 3% (v/v) HNO_3 to yield final solutions with U concentrations ranging from 50 to 100 ppb.

Trace element concentrations were measured at the Leibniz University Hannover using a Thermo Scientific Element XR high-resolution ICP-MS (HR-ICP-MS) in 'triple' detector mode using the low and medium-resolution modes ($M/\Delta M_{MR} \approx 4{,}000$). Prior to starting measurements, the instrument was tuned using Li, In and U and UOx to maximum signal sensitivity and stability whilst maintaining the oxide formation rate below 5%. A five-point external calibration procedure using multi-element standard solutions containing the target elements (Al, Mn, Fe, Sr, Th and ^{238}U) with concentrations ranging from 0 to 50 μg/L was used to quantify the concentrations. Instrument drift during measurements was monitored using rhodium-103 as an internal standard. The lake water standard TMDA-51.3 was measured repeatedly to ensure accuracy and precision were less than ±10%.

Uranium isotope measurements were conducted using a Thermo Scientific™ Neptune Plus™ in low-resolution mode at LUH with a Cetac Aridus 2 sample introduction system (dry plasma conditions) following Noordmann et al. (2015). A standard Ni H sampler cone and X skimmer cone were used. The U sensitivity of this setup achieved >1 V/ppb sensitivity. The ^{233}U, ^{235}U and ^{236}U isotopes were measured using Faraday detectors with 10^{11} Ω resistors, ^{238}U was measured with a 10^{10} Ω resistor and ^{234}U isotope was measured with a 10^{13} Ω resistor. The abundance sensitivity of ^{238}U on ^{236}U was monitored to ensure it was <1 ppm. Instrumental mass bias was corrected using the $^{233}U/^{236}U$ ratio according to the exponential law. Measurement sequences were performed using a standard-sample-bracketing method relative to a CRM-112A standard solution to calculate $\delta^{238}U$ (Eq. (1)) and $\delta^{234}U$ were calculated relative to the secular equilibrium (SE) ratio of $^{234}U/^{238}U = 54.891 \pm 0.094 \times 10^{6}$ (2 s.d.; Cheng et al., 2000). Uranium isotope ratios are reported according to convention using delta notation (in ‰), given by the following equations:

$$\delta^{238}U = \left[\left({}^{238}U/{}^{235}U \right)_{sample} / \left({}^{238}U/{}^{235}U \right)_{CRM112A} - 1 \right] * 1000 \quad (1)$$

$$\delta^{234}U = \left[\left({}^{234}U/{}^{238}U \right)_{sample} / \left({}^{234}U/{}^{238}U \right)_{s.e.} - 1 \right] * 1000 \quad (2)$$

All δ-values of samples represent triplicate measurements where uncertainty values represent 2σ standard error (2 s.e.) for both $\delta^{238}U$ and $\delta^{234}U$. Reference materials were measured repeatedly before, after and throughout the sequence to monitor the instrument performance and a limestone (JLs; Geological Survey of Japan) was also processed with each batch of samples for column chromatography. The average $\delta^{238}U$ values of IRMM-184, Reimep-18a and JLs were −1.19 ± 0.09‰ (2 s.d., n = 12), −0.27 ± 0.09‰ (2 s.d., n = 10), and −0.24 ± 0.10‰ (2 s.d., n = 7), respectively, and their average $\delta^{234}U$ values were −27.6 ± 2.1‰, 35.1 ± 3.0‰, and 5.7 ± 2.0‰. All measured values are consistent with previously reported values (Richter et al., 2005; Weyer et al., 2008; Richter et al., 2010; Asael et al., 2013; Albut et al., 2019; Brüske et al., 2020a). Total procedural blanks from leaching and column chromatography were <4 ng and no blank corrections were applied to the data. The U content of the gypseous plaster was 11 ppb, but this material was avoided during sampling the inner areas of SBS-1 and SBS-2 and not detected in XRD measurements. Thus, it likely comprised <1 wt% of sample powders (according to the approximate XRD detection limit) and likely contributed much <0.1 ng of U to sample measurements.

5. Results

5.1. Hydrochemistry and water stable-isotope compositions

Two seawater samples and one groundwater sample were collected from Shark Bay in 2019. Both seawater samples were hypersaline (59.8–65.6 PSU) and within the range of typical values for Shark Bay (40 to ~75 PSU) that vary according to the season and the distance from the Faure Sill (Jahnert and Collins, 2012; Suosaari et al., 2016), which restricts inflow of seawater into Hamelin Pool (Fig. 1). The evaporitic conditions at Shark Bay are also reflected in the higher measured $\delta^{18}O$ and $\delta^{2}H$ of +3.8 to +4.3‰ and +24.1 and +26.4‰, respectively (Table 1). The seawater was fully oxic (ORP: 200 mV) at the time of sampling (roughly midday), as expected from the diurnal cycle of high oxygen concentrations in the daytime due to high photosynthesis rates and lower oxygen concentrations at night (Jahnert and Collins, 2012; Wong et al., 2015). In contrast to seawater samples, the groundwater sample was less saline (3.6 PSU, i.e., brackish), more reduced (ORP = 93 mV), and had a lower $\delta^{18}O$ (−5.3‰), which is typical for meteoric groundwaters draining carbonate aeolianite (Tamala Limestone) aquifers in Western Australia (Bryan et al., 2016). The total alkalinity of the seawater samples (130 and 132 mg/l) were higher than open marine seawater (~120 mg/l). This may be attributed to the inflow of high-alkalinity groundwater (214 mg/l) from the carbonate aquifer around Shark Bay.

The U concentrations in the two Shark Bay seawater samples and the collected groundwater sample were 10.9, 11.1 and 6.2 μg/l, respectively (Table 1). Adopting an average seawater value of 3.3 μg/l (U/Cl = 0.2 μg/g; Weyer et al., 2008), the U concentration in Shark Bay seawater (U/Cl = 0.3 μg/g) is slightly higher than would be expected for the conservative enrichment of U by evapo-concentration effects. This may be because the seawater was sampled from the shoreline in Hamelin Pool. Moreover, the relatively high U concentration in the brackish groundwater sample (U/Cl = 3.0 μg/g) might point toward carbonate dissolution within the Tamala Limestone aquifer as an additional, local source of U via submarine groundwater discharge, in addition to alkalinity that facilitates stromatolite growth. Constraining the dynamics of groundwater–seawater interactions would require additional sampling and is beyond the scope of this study, but these data support arguments that stromatolite occurrence is linked to carbonate seawater chemistry.

Shark Bay seawater exhibited $\delta^{238}U$ values of −0.36 ± 0.02 and −0.37 ± 0.02‰ (Table 1), which are similar to the global average for open seawater (−0.39 ± 0.04‰; 1 s.d.; see our literature compilation in Table A.1). Likewise, the Shark Bay seawater samples exhibited similar $\delta^{234}U$ values (+146.8 ± 1.4 and + 143.5 ± 1.0‰) relative to open seawater (+146.7 ± 3.6‰; Table A.1). The groundwater sample exhibited both higher $\delta^{238}U$ and $\delta^{234}U$ (−0.19 ± 0.03‰ and + 732.8 ± 0.8, respectively) compared to the seawater samples, likely due to increased water–rock interactions in the aquifer.

5.2. Mineralogical, organic carbon, and stable isotope composition of Shark Bay stromatolites

Qualitative XRD data for the modern stromatolite crusts show that they primarily comprise aragonite with minor proportions of calcite and quartz (Fig. S1). Quantitative XRD data for SBS-1 and SBS-2 reveal that the major aragonite component represents ~90 wt% of the stromatolite material (Table 3). These data are consistent with previous findings that microbial carbonate (micrite) precipitated in Shark Bay stromatolites is predominantly aragonite (Reid et al., 2003; Jahnert and Collins, 2012; Suosaari et al., 2016).

Table 3
Organic carbon and quantitative XRD mineralogy data for stromatolites SBS-1 and SBS-2.

Sample ID	Organic C	Mineralogy		
		Aragonite	Quartz	Calcite
	(wt.%)	(wt.%)	(wt.%)	(wt.%)
SBS-1A (top)	0.8	94	1	5
SBS-1B	0.6	94	2	4
SBS-1C	0.6	94	2	4
SBS-1D	0.5	91	2	7
SBS-1E	0.5	92	2	6
SBS-1F	0.4	91	2	7
SBS-1G (sub.)	0.1	0	0	100
SBS-2A (top)	NA	90	3	8
SBS-2B	NA	90	2	8
SBS-2C	NA	92	4	4
SBS-2D	NA	93	4	4
SBS-2E	NA	91	4	4
SBS-2F	NA	91	5	4
SBS-2G	NA	91	3	6
SBS-2H (sub.)	NA	91	3	6

Where "top" and "sub" indicate the top and substrate of each stromatolite, with results displayed in sequential order from the uppermost lamina to the base. TOC analyses by Amdel Laboratory, Adelaide, 1984. XRD mineralogy at Research School of Earth Sciences, Australian National University. Small amounts of kaolinite and mica (~1%) were detected by XRD, but were too low to be reliably quantified. NA: not analysed.

The organic carbon (OC) content of SBS-1 ranged from 0.8 to 0.1%, with the lowest OC found in the substrate, SBS-1-G (Table 3).

The seven modern stromatolite crusts exhibited $\delta^{18}O$ values from +2.9 to +3.4‰ (Table 4), which is consistent with the highly evaporative conditions in modern Shark Bay and the range of previous measurements (+3.1 to +3.9‰; Jahnert and Collins, 2012). The $\delta^{18}O$ of the older stromatolite material from SBS-1 and SBS-2 ranged from +0.5 to 3.6‰ and +1.2 to +3.2‰, respectively. The anomalously low value for SBS-1-G (+0.5‰) is expected because this sample represents indurated substrate material (a dense carbonate pebble) upon which the stromatolite grew. Excluding this substrate material, the higher $\delta^{18}O$ of the other samples demonstrate that the evaporative conditions found in the modern environment have persisted throughout the growth history of SBS-1 and SBS-2 (~1 ka; Chivas et al., 1990).

The $\delta^{13}C$ values from modern stromatolite crusts (+5.2 to +6.0‰; Table 4) overlap with strongly positive $\delta^{13}C$ values of SBS-1 and SBS-2 (+3.8 to +5.9‰) that were previously measured by Chivas et al. (1990) – excluding the substrate sample SBS-1-G that displays a lower $\delta^{13}C$ (−1.5‰). The correlation between $\delta^{13}C$ and $\delta^{18}O$ values (r = 0.69) is a common feature of shallow carbonate platforms, such as Shark Bay and the Bahamas (Geyman and Maloof, 2019).

5.3. Leaching experiments on modern stromatolites

A range of acids, similar to those tested by Clarkson et al. (2020), were reacted with a Shark Bay stromatolite powder (SB19-2-2x) at room temperature for 1 or 24 h (see Table 2 for details). The use of 1 M NH_4Ac was also tested but excluded from further U isotope investigations on this basis of the low amount of U extracted. The optimum acid for selectively leaching the microbial carbonate fraction in modern stromatolites was evaluated in terms of the concentrations of elements associated with detrital silicates (Al and Th) and Fe oxy(hydroxides) (Fe and Mn) in leachates, which should ideally be minimised.

Leaching using 0.2 M AcOH yielded the lowest concentrations of Al, Th and Fe in the leachates compared to HCl and HNO_3 (Table 2). For instance, compared to 0.2 M AcOH, leaching using 0.5 M HCl increased the Al, Fe and Th concentrations by factors of ~2.5, ~5, and ~2.5, respectively. This could be attributed to the lower pH of strong acid solutions at both the start and end of experiments, e.g., a pH < 1.2 for HNO_3 and HCl solutions compared to pH > 2.3 for 0.2 M AcOH (Table 2). Interestingly, however, there was no difference in Mn concentrations between AcOH, HCl and HNO_3 leachates. The use of a 1 M NaOAc/AcOH solution buffered at pH 5 yielded similar concentrations of Al and Fe compared to 0.2 M AcOH (Table 2). This might suggest the use of a buffer is unnecessary when leaching carbonate materials, e.g., stromatolites, due to the strong buffering effect of released CO_3^{2-}, as demonstrated by the relatively high final pH (>5.6) of all AcOH leaching solutions.

More U was generally extracted in experiments conducted for 24 h compared to 1 h without any concomitant increase in Al or Fe concentrations for 0.2 M AcOH (Table 2). The greater amount of starting material dissolved after 24 h suggests that a longer reaction time may be preferable for the slow reaction kinetics when dissolving carbonates using weak dilute acids, such as 0.2 M AcOH. Similarly, longer reaction times when using HCl and HNO_3 extracted more U, but, unlike for AcOH, this was associated with a ~50% increase in Al and Fe concentrations (Table 2).

Despite clear differences in the elemental concentrations found in leachates, the U isotope composition of leachates were similar, ranging from −0.31 ± 0.03‰ to −0.33 ± 0.01‰ for $\delta^{238}U$ and +14 8.1 ± 0.1‰ to +150.6 ± 0.2‰ for $\delta^{234}U$ (Table 2). Although all measurements yielded identical results within analytical error, the average $\delta^{238}U$ for the AcOH leachates (−0.32 ± <0.01‰, 2.s.d,

Table 4
Trace element, stable isotope and U isotope composition of stromatolites from Shark Bay.

Sample ID	Tidal zone	Al µg/g	Mn µg/g	Fe µg/g	U µg/g	Th/U wt./wt.	$\delta^{13}C_{VPDB}$ ‰	$\delta^{18}O_{VPDB}$ ‰	$\delta^{238}U$ ‰		2 s.e. ‰	$\delta^{234}U$ ‰		2 s.e. ‰
SB19-1-2	Intertidal	11.7	1.6	3.5	0.31	0.02	5.2	3.4	−0.32	±	0.01	150.9	±	0.6
SB19-1-3a	Intertidal	14.6	3.2	5.1	0.28	0.02	5.6	3.4	−0.30	±	0.11	149.2	±	0.4
SB19-1-3b	Intertidal	13.9	10.4	13.8	0.53	0.01	5.6	3.2	−0.33	±	0.10	149.3	±	0.9
SB19-1-4	Intertidal	13.1	1.2	2.1	0.36	0.02	5.8	3.5	−0.33	±	0.06	151.1	±	1.0
SB19-2-2x	Subtidal	13.3	5.8	7.5	0.57	0.02	6.0	3.4	−0.30	±	0.07	150.0	±	0.4
SB-3-1	Supratidal	14.9	3.2	4.2	1.10	<0.010	5.3	2.9	−0.43	±	0.03	156.7	±	2.6
SB19-3-2	Supratidal	12.8	2.3	6.2	0.64	0.012	5.8	3.1	−0.16	±	0.04	156.1	±	0.1
SBS-1A (top)	Subtidal	46.3	3.5	5.6	0.90	0.10	5.0	1.9	−0.29	±	0.01	152.9	±	1.3
SBS-1B	Subtidal	32.8	3.1	4.0	0.97	0.10	5.1	1.8	−0.31	±	0.08	154.6	±	0.1
SBS-1C	Subtidal	22.9	3.8	4.4	1.00	0.11	5.3	2.8	−0.22	±	0.07	153.8	±	0.5
SBS-1D	Subtidal	34.3	4.3	6.5	0.85	0.10	5.3	3.6	−0.19	±	0.05	151.6	±	0.5
SBS-1E	Subtidal	15.8	4.8	5.3	0.77	0.11	4.3	0.9	−0.18	±	0.02	150.6	±	1.2
SBS-1F	Subtidal	34.4	5.2	5.6	0.92	0.12	5.2	3.8	−0.21	±	0.07	148.5	±	0.5
SBS-1G (sub.)	Subtidal	19.7	52.9	18.0	1.80	0.05	−1.5	0.5	+0.11	±	0.12	157.1	±	1.0
SBS-2A (top)	Intertidal	23.7	5.4	5.4	0.89	0.09	5.0	3.2	−0.15	±	0.02	148.1	±	0.5
SBS-2B	Intertidal	29.7	5.5	7.1	0.96	0.09	4.7	2.5	−0.15	±	0.05	147.4	±	1.3
SBS-2C	Intertidal	51.0	4.1	5.2	1.02	0.09	4.4	1.9	−0.29	±	0.04	148.5	±	1.9
SBS-2D	Intertidal	16.1	2.8	1.8	0.63	0.09	5.0	3.2	−0.30	±	0.13	148.9	±	0.4
SBS-2E	Intertidal	24.3	3.8	4.4	0.91	0.09	5.0	3.2	−0.33	±	0.10	147.7	±	0.9
SBS-2F	Intertidal	19.5	4.6	4.1	0.88	0.10	4.7	2.0	−0.32	±	0.03	148.3	±	0.4
SBS-2G	Intertidal	46.3	4.6	4.7	0.97	0.10	4.1	1.1	−0.29	±	0.09	148.8	±	0.4
SBS-2H (sub.)	Intertidal	32.8	3.3	2.3	0.59	0.09	4.8	3.1	−0.33	±	0.12	147.9	±	0.7

Where "top" and "sub" indicate the top and substrate of each stromatolite, with results displayed in sequential order from the uppermost lamina to the base. The $\delta^{13}C$ and $\delta^{18}O$ data for stromatolites SBS-1 and SBS-2 derive from Chivas' laboratory at the Australian National University.

n = 4) were significantly lower (p = 0.03, two-tail *t* test) than for the HCl and HNO_3 leachates (−0.34 ± 0.00‰, 2 s.d., n = 6). In our study, the use of 0.2 M AcOH was preferred to 1 M NaOAc/AcOH solution due to the anomalously high Th/U ratio for NaOAc/AcOH leachates compared to AcOH (Th/U: 1.36 vs 0.04; Table 2), and the increased load of Na on the resin during column chromatography for 1 M NaOAc/AcOH leachates. A 24 h reaction duration was preferred to 1 h for 0.2 M AcOH because the proportion of starting material dissolved increased from 53 to 64 wt% with no concurrent increase in Al, Fe and Th concentrations, and the 0.2 M AcOH leachates yielded identical $\delta^{238}U$ values. Thus, all stromatolite samples were leached using 0.2 M AcOH for 24 h at room temperature. It is expected that the U in the AcOH leaches is sourced from both the primary crystal lattice framework of aragonite crystals and any secondary carbonate cements present.

5.4. Trace element compositions of modern stromatolites

The trace element and U isotope data for the leached modern stromatolite crusts, and older stromatolite material from SBS-1 and SBS-2 are given in Table 4 (see Table S2 for correlation matrices). Student's *t*-test method (two-tail assuming unequal variance of sample observations) was used for all statistical significance tests to calculate p-values. A p-value threshold of 0.05 was taken to reject the null hypothesis in favour of the alternative hypothesis.

The U concentrations of the modern stromatolite crusts ranged from 0.28 to 1.13 µg/g, with an average of 0.55 ± 0.29 µg/g (1 s.d., n = 7; Fig. 3A), whereas the U concentrations of the older material from SBS-1 and SBS-2 ranged from 0.59 to 1.82 µg/g (average: 0.94 ± 0.35 µg/g) and were significantly higher than the modern crusts (p = 0.01). However, there was no significant difference between the U concentrations in SBS-1 and SBS-2 (p = 0.25). All Th/U ratios were very low (<0.12) relative to the crustal average ($Th/U_{crustal} \approx 4$) and all Al concentrations were also low (<50 µg/g; Fig. 3B). These parameters are both indicators for detrital contamination in carbonates and Th/U ratios and Al concentrations correlate in all samples (r = 0.65). Interestingly, this correlation was much stronger in the modern stromatolite crusts (r = 0.96) than in SBS-1 (r = 0.27) and SBS-2 (r = 0.12). Despite the lack of correlation between Th/U and Al in the older stromatolite material, both Th/U ratios and Al contents were significantly higher (p < 0.01) for SBS-1 and SBS-2 compared to the modern stromatolite crusts.

The Mn and Fe contents of all stromatolites ranged from 1.6 to 10.4 µg/g and 1.8 to 13.8 µg/g, respectively, excluding the substrate material (SBS-1G) that contains anomalously high Mn and Fe contents of 52.9 and 18 µg/g, respectively (Fig. 3C). The Mn and Fe contents correlate highly in all samples (r = 0.84). There were no significant differences between the modern crusts and SBS-1/SBS-2 in terms of their Mn (p = 0.81) and Fe concentrations (p = 0.33). The U contents also correlated with the Mn (r = 0.69; Fig. 3D) and Fe contents (r = 0.84).

5.5. Uranium isotope compositions of modern stromatolites

The $\delta^{238}U$ of all stromatolite samples ranged from –0.43 ± 0.03 to +0.11 ± 0.12‰ (Table 4; Fig. 4A). The stromatolite crusts from the intertidal and subtidal sites (SB19-1 and SB19-2) exhibited indistinguishable $\delta^{238}U$ values (−0.30 ± 0.07 to −0.33 ± 0.10‰, n = 5), which are slightly higher than the average value for Shark Bay seawater (−0.37 ± 0.02‰; Table 1). More variable $\delta^{238}U$ values from −0.16 ± 0.04 to −0.43 ± 0.03 were found for the supratidal microbial pavement samples (SB19-3–1 and SB19-3–2; Table 4). The $\delta^{238}U$ of older, deeper laminae from SBS-1 and SBS-2 varied from ca. −0.3‰ up to −0.2‰ in SBS-1 and SBS-2. These $\delta^{238}U$ values are significantly higher than Shark Bay seawater (Table 1), and modern crusts from the subtidal and intertidal zones (p = 0.01). The substrate material upon which stromatolite SBS-1 grew (SBS-1G) exhibited the highest $\delta^{238}U$ value (+0.11 ± 0.12‰) in our study. This is unsurprising as this material is not likely related to stromatolite growth, as evidenced by the lower $\delta^{13}C$ and $\delta^{18}O$ values and the calcitic versus aragonitic mineralogy of this sample compared to stromatolite material (Chivas et al., 1990). Relative to $\delta^{238}U$, less variation was found in the $\delta^{234}U$ of stromatolite samples (Fig. 4B), with an average of +150.8 ± 3.1‰ (1 s.d.), which is similar to – but slightly higher than – the average $\delta^{234}U$ of seawater (+146.7 ± 3.6‰; Table A.1). Similarly high $\delta^{234}U$ up to +157.1 ± 1.0 were also measured in SBS-1, but not SBS-2 (Table 4).

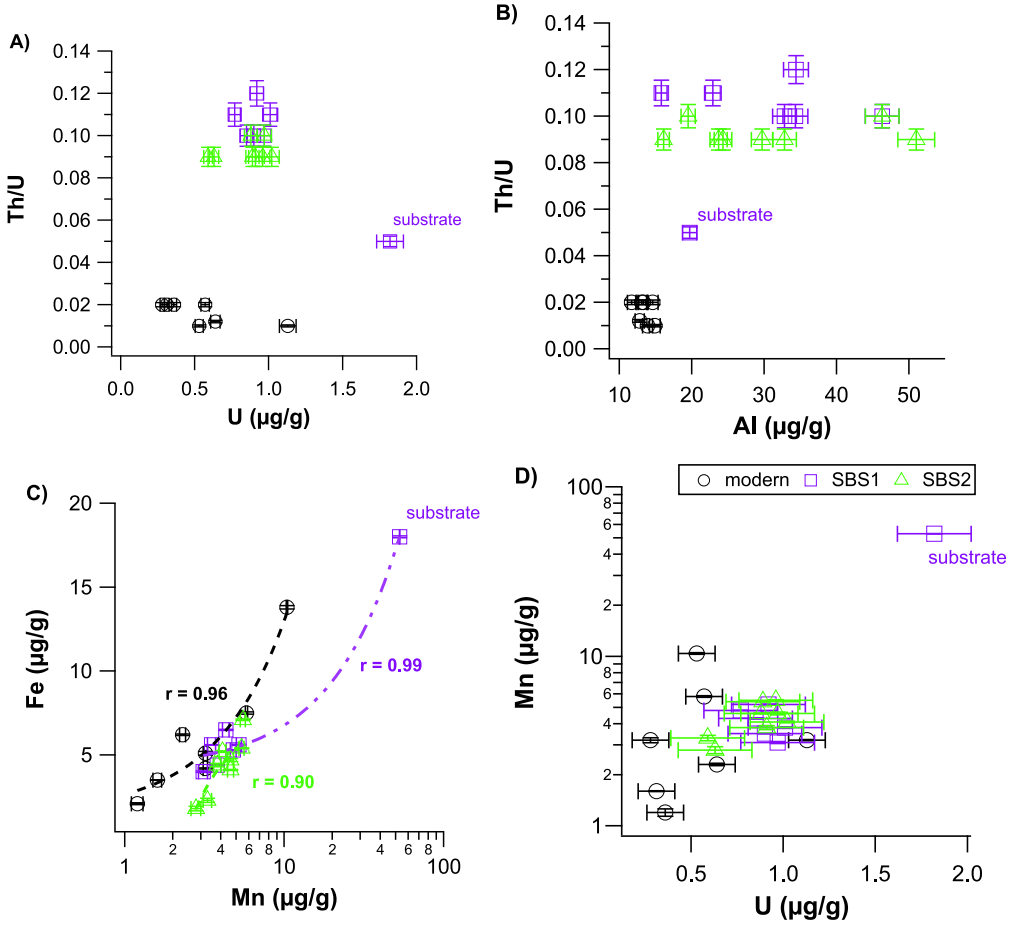

Fig. 3. Plots of (A) Th/U vs U contents, (B) Th/U vs Al contents, (C) Fe vs Mn contents, (D) Mn vs U contents in Shark Bay stromatolites. Modern crusts, SBS-1 and SBS-2 samples are shown by black open circles, purple open squares, and green open triangles, respectively. (For interpretation of the references to colour in this figure legend, the reader is referred to the web version of this article.)

When considering all data from modern stromatolite crusts and SBS-1/SBS-2, there was a correlation between $\delta^{238}U$ and Mn (r = 0.75), Fe (r = 0.65) and U concentrations (r = 0.58), and an apparent negative correlation with $\delta^{13}C$ (Table A.2; Fig. S2). No correlations were found between $\delta^{238}U$ and $\delta^{234}U$ (Fig. 4C), or any other parameter when considering all stromatolite data. However, there was a correlation between $\delta^{234}U$ and the U content for the modern stromatolite crusts (r = 0.75) and SBS-1 (r = 0.76).

6. Discussion

6.1. Variations of $\delta^{238}U$ in modern aragonitic crusts of stromatolites from the subtidal and intertidal zones in Hamelin Pool

The low gradient of Hamelin Pool provides a variety of tidal environments for stromatolite development and although the microbial habitats in Hamelin Pool are highly variable, they may be broadly simplified into three main zones: subtidal, intertidal and supratidal. The role of tidal environment in controlling the trace element and U isotope composition is discussed in the following.

Modern stromatolite crusts from the subtidal and intertidal zones exhibited a very narrow range of $\delta^{238}U$ (average: −0.32 ± 0.02‰; 1 s.d.) that appear to be systematically offset from seawater. This range is slightly higher than other primary carbonate precipitates that form in shallow-marine environments, which typically yield $\delta^{238}U$ closer to modern seawater (Fig. 5; Stirling et al., 2007; Weyer et al., 2008; Romaniello et al., 2013; Tissot and Dauphas, 2015; Chen et al., 2018b; Kipp et al., 2022a). The exception to this is molluscs, which can be distinguished by their low U concentrations (ca. 0.05 µg/g) and calcitic mineralogy in contrast to aragonitic corals (2.5–3.5 µg/g U) and modern aragonitic crusts of stromatolites (0.3–1.1 µg/g).

The higher $\delta^{238}U$ value measured for the modern stromatolite crusts is closer to the predicted value for the precipitation of aragonite from seawater ($\alpha_{CaCO3\text{-}SW}$: 1.00009–1.00013) and we explore if this mechanism could explain the observed seawater offset in modern stromatolite crusts from Shark Bay in the following. Chen et al. (2016) proposed that equilibrium fractionation among different aqueous U species and preferential incorporation of isotopically heavy U species into aragonite is the most likely mechanism driving U isotope fractionation, rather than a change in coordination state of U during aragonite precipitation. Based on the general observation that species with lower coordination numbers and shorter bond lengths typically favour the incorporation of heavier isotopes, Chen et al. (2016) also predicted that the dissolved U species $Ca_2UO_2(CO_3)_3$ and $UO_2(CO_3)_3^{4-}$ are likely to be isotopically lighter than $CaUO_2(CO_3)_3^{2-}$ and $MgUO_2(CO_3)_3^{2-}$ (see Table S3 for bond lengths and coordination numbers of aqueous U species). Thus, the key variables controlling the U isotope composition of precipitated aragonite are the proportion of dissolved U present as the aqueous species $Ca_2UO_2(CO_3)_3$ and $MgUO_2(CO_3)_3^{2-}$.

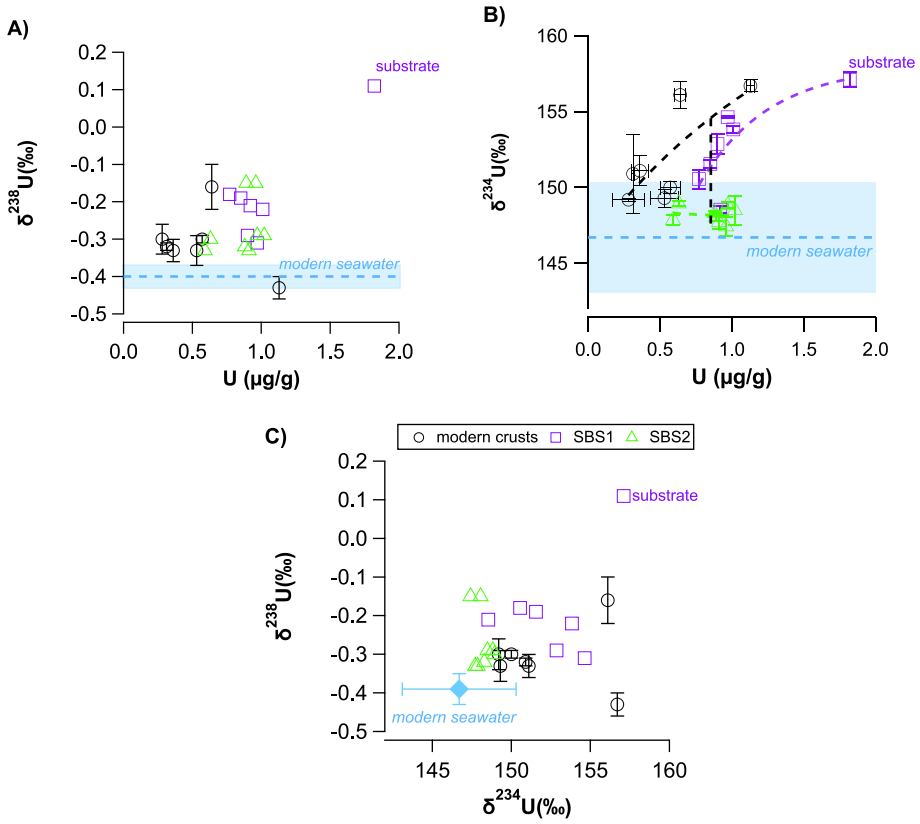

Fig. 4. Plots of (A) $\delta^{238}U$ vs U contents, (B) $\delta^{234}U$ vs U contents and, (C) $\delta^{238}U$ vs $\delta^{234}U$ in Shark Bay stromatolites. Modern crusts, SBS-1 and SBS-2 samples are shown by black open circles, purple squares, and green triangles, respectively. The blue dashed line shows the average $\delta^{238}U$ and $\delta^{234}U$ values for modern seawater whereby the shaded blue area represents 1σ standard deviation around the mean, except in (C) where these data are represented by a marker and error bars (compiled data in Table S1). (For interpretation of the references to colour in this figure legend, the reader is referred to the web version of this article.)

To quantitatively assess the potential effect of $Ca_2UO_2(CO_3)_3$ and $MgUO_2(CO_3)_3^{2-}$ species on U isotope fractionation during aragonite precipitation from hypersaline Shark Bay seawater, we modelled the speciation of U compared to open marine seawater using PHREEQC version 3 (Parkhurst and Appelo, 2013). Following Chen et al. (2017), we used the PHREEQC database "sit.dat" to employ the specific ion interaction theory (SIT) that is appropriate for high salinity, NaCl-dominated solutions and includes updated thermodynamic data for U (Grenthe et al., 1992; Guillaumont and Mompean, 2003). We supplemented this database with updated thermodynamic data for $Ca_2UO_2(CO_3)_3$, $CaUO_2(CO_3)_2^{3-}$, and $MgUO_2(CO_3)_2^{3-}$, which are important aqueous U species in seawater (Dong and Brooks, 2006). Indeed, our aqueous speciation modelling results confirm that there is a higher proportion of U present as $Ca_2UO_2(CO_3)_3$ in hypersaline Shark Bay seawater relative to open marine seawater (58 vs 42%; Table S3).

The higher fraction of neutrally charged U species in Shark Bay seawater should lead to a larger U isotope fractionation factor for aragonite precipitation, however, the modern aragonitic crusts of stromatolites did not exhibit more U isotope fractionation than the abiotic aragonite coprecipitation experiments. To further explore this quantitively, we estimated the isotope fractionation factor (α) for aragonite precipitation in Shark Bay seawater using the speciation-dependent isotope fractionation equation derived by Chen et al. (2016), given as:

$$\alpha = \frac{^{238}U_{2-1}}{1000}\frac{(f_{neutral})^2}{f_{neutral}-1}\left(1+\frac{K_1}{K_2}\times\frac{1}{\gamma_{UO_2(CO_3)_3^{4-}}\gamma_{Ca^{2+}}[Ca^{2+}]}\right)+1 \quad (3)$$

where γi is activity coefficient of chemical species and chemical species in square brackets represent the concentration of those species (e.g., $[Ca^{2+}]$ is the Ca^{2+} concentration). The proportion of neutral U species in Shark Bay seawater was calculated in PHREEQC as previously described ($f_{neutral}$ = 0.58; Table S3). Following Chen et al. (2016), the activity coefficient of the neutral U species $Ca_2UO_2(CO_3)_3$(aq) is assumed to be 1 and the value of $\Delta^{238}U_{2-1}$ is inferred to be 0.32 ± 0.06‰, where Group 1 refers to the aqueous U species $UO_2(CO_3)_3^{4-}$ and $Ca_2UO_2(CO_3)_3$ and Group 2 refers to $CaUO_2(CO_3)_3^{2-}$ and $MgUO_2(CO_3)_3^{2-}$. The respective equilibrium constants, K_1 and K_2, for the aqueous U species $UO_2(CO_3)_3^{4-}$ and $Ca_2UO_2(CO_3)_3$ are given as (Chen et al., 2016):

$$K_1 = \frac{\gamma_{UO_2(CO_3)_3^{4-}}[UO_2(CO_3)_3^{4-}]}{(\gamma_{UO_2^{2+}}[UO_2^{2+}])(\gamma_{CO_3^{2-}}[CO_3^{2-}])^3} \quad (4)$$

$$K_2 = \frac{\gamma_{Ca_2UO_2(CO_3)_3}[Ca_2UO_2(CO_3)_3]}{(\gamma_{UO_2^{2+}}[UO_2^{2+}])(\gamma_{CO_3^{2-}}[CO_3^{2-}])^3(\gamma_{Ca^{2+}}[Ca^{2+}])} \quad (5)$$

where all parameters are defined the same as those in Eqs. (3) and (4) and Chen et al. (2016). Following this approach, the isotope fractionation is predicted to be α = 1.00026. Assuming that $\varepsilon_{A\text{-}B} = (\alpha_{A\text{-}B} - 1)\cdot 1000$ and $\varepsilon_{A\text{-}B} \approx \delta_A - \delta_B$, the offset of +0.05 to +0.07‰ in modern aragonitic crusts of stromatolites is much less than would be predicted for primary aragonite precipitation in Shark Bay seawater. As suggested by Chen et al. (2016), the limited expression of U isotope fractionation in primary marine carbonate precipitates may be related to the local concentrations of Mg^{2+}, Ca^{2+}, and CO_3^{2-}, and/or pH at biologically (microbially) mediated or influenced calcification sites.

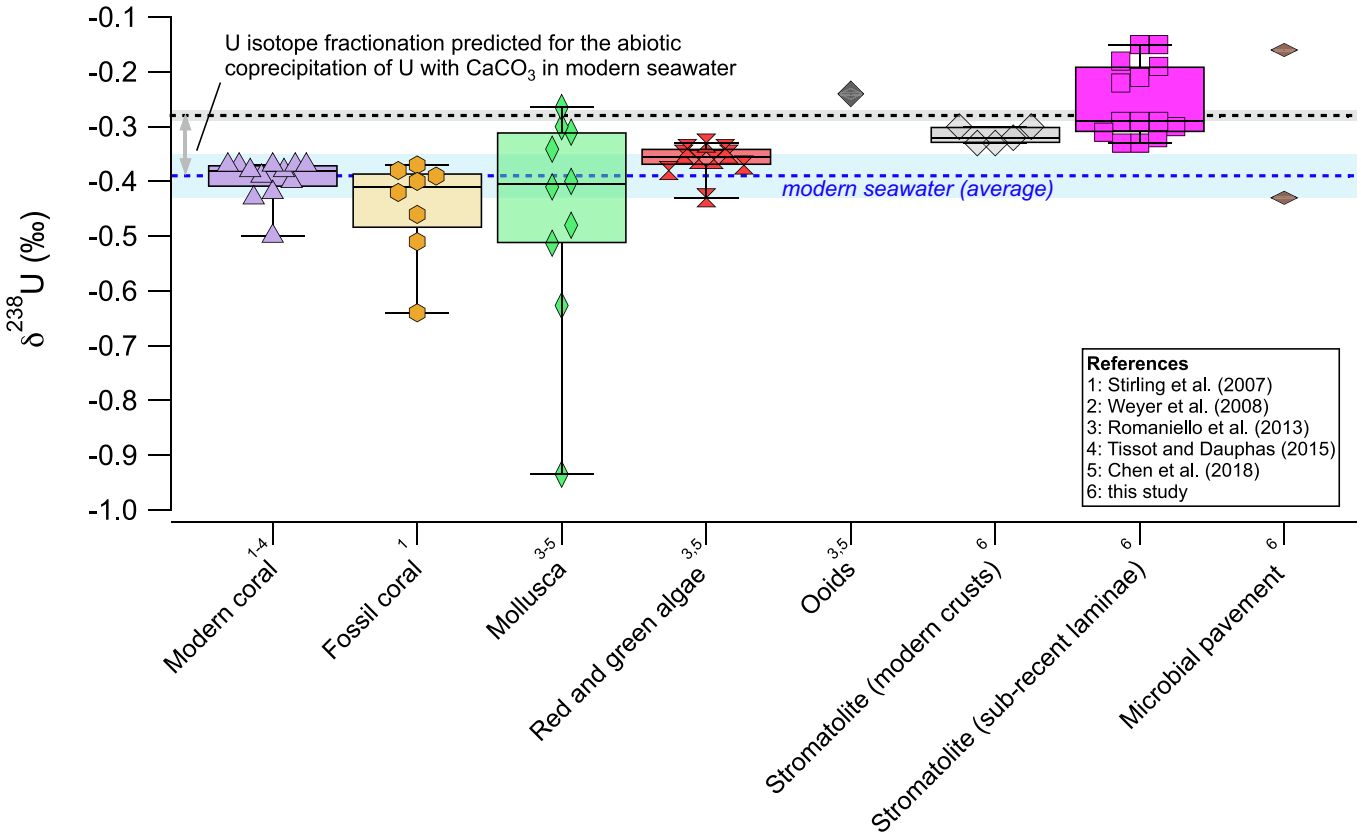

Fig. 5. Box plots showing the distribution of $\delta^{238}U$ values for primary carbonate precipitates from modern shallow-marine environments. Markers represent individual sample measurements including data from this study and the literature (Stirling et al., 2007; Weyer et al., 2008; Romaniello et al., 2013; Chen et al., 2018b; Tissot et al., 2018) Romaniello et al. (2013) and Chen et al. (2018b). The blue dashed line shows the average $\delta^{238}U$ value for modern seawater and the shaded blue area represents 1σ standard deviation around the mean (compiled data in Table S1). The dashed black line shows the predicted value for an aragonitic carbonate that is abiotically precipitated from modern seawater according to experimental data from Chen et al. (2016) where the grey shaded area indicates the uncertainty according to the propagated error. (For interpretation of the references to colour in this figure legend, the reader is referred to the web version of this article.)

6.2. Is microbial pavement a reliable archive of $\delta^{238}U$?

Microbial pavement is an important feature in Hamelin Pool and covers over 200 km^2 of the present subtidal surface (Jahnert and Collins, 2012), but the wide range of $\delta^{238}U$ values (−0.43 ± 0.03 and −0.16 ± 0.04‰) for the two microbial pavement samples, which are now exposed in the supratidal zone, suggest that these microbial deposits are not a reliable archive of $\delta^{238}U$. This could be because the microbial pavement currently found in the modern supratidal zone likely began forming when the sea level was higher between 2,000 and 1,100 years ago (Chivas et al., 1990; Jahnert and Collins, 2012). Thus, these microbial carbonate precipitates are likely much older than the modern aragonitic crusts of stromatolites and have likely undergone some diagenesis in shallow-marine and subaerial environments. A role for authigenic U accumulation is supported by twofold higher average U contents of microbial pavement samples compared to modern aragonitic crusts of stromatolites (0.9 vs 0.4 μg/g) and the higher $\delta^{234}U$ of the microbial pavement samples (+156‰ vs +150‰). Interestingly, U enrichment occurred in both samples without any concurrent enrichment in Fe, Mn, Al or Th (Table 4), which are typical markers of diagenetic alteration or detrital contamination. Likewise, no correlation was found between $\delta^{238}U$ with U concentrations, or other common diagenetic indicators, in carbonate sediments from the Bahamas (Romaniello et al., 2013; Chen et al., 2018a). Moreover, assuming that the primary $\delta^{238}U$ signature of the supratidal microbial pavement was similar to that of the modern aragonitic crusts of stromatolites, their $\delta^{238}U$ have been modified in different directions from ca. −0.32‰ to −0.43‰ and −0.16‰, respectively. Given the preferential reduction of ^{238}U, the $\delta^{238}U$ value of −0.16‰ might suggest that authigenic U in the sample was accumulated under reducing conditions, whereas authigenic U accumulation occurred under oxic conditions in a microbial pavement sample with a seawater-like value of −0.43‰. Further work and a larger dataset is clearly required to better understand U accumulation and U isotope fractionation processes in microbial pavement.

6.3. The evolution of $\delta^{238}U$ in older stromatolite laminae

The higher $\delta^{238}U$ of the older (sub-recent) laminae from SBS-1 and SBS-2 (up to −0.15 ± 0.05‰) suggest that the near-primary $\delta^{238}U$ signature of seawater recorded in modern aragonitic crusts of stromatolite (see Section 6.1) is rapidly altered (<1 ka) due to the preferential accumulation of ^{238}U under reducing conditions in the more-cemented, older stromatolite laminae. Firstly, the preferential reduction of ^{238}U relative to ^{235}U caused by the nuclear field shift effect is well established (Stirling et al., 2007; Weyer et al., 2008; Andersen et al., 2017; Brüske et al., 2020b). Moreover, the oxic zone in microbial mats on stromatolite surfaces at Shark Bay is limited to the upper 0 to 4 mm depth, where the majority of cyanobacteria reside and oxygenic photosynthesis occurs, i.e. the photic zone, whereas anoxic conditions prevail below ~5 mm depth (Wong et al., 2015). This yields an inverse relationship between oxygen and sulfide concentrations, whereby the latter increases to around 250 μM below 5 mm depth and similar sulfide concentrations were measured in carbonate platform core sediments in the Bahamas, which also exhibited significant U isotope offsets from seawater (Romaniello et al., 2013). We propose that

the host phase for authigenic U precipitated from reducing pore fluids is the micritic cement that infills porosity present within the primary stromatolite structure, which is expected for SBS-1 and SBS-2 as they are laminated calcarenite stromatolites that formed in the subtidal-intertidal zone at Shark Bay (Reid et al., 2003). A similar process would be expected to occur in laminated calcarenite stromatolites from the Bahamas that exhibit a similar structure. Radiocarbon dating reveals that this U alteration process has occurred within 690 ± 60 and 490 ± 115 cal years BP for SBS-1 and SBS-2, respectively (Chivas et al., 1990). As many U isotope studies of stromatolites are interested in million-to-billion-year timescales, the onset of this alteration process within 1,000 years can essentially be considered syndepositional.

Similarly high $\delta^{238}U$ values were found in bulk carbonate sediments from the Bahamas, which were also offset from seawater by +0.2 to +0.4‰ (Romaniello et al., 2013; Chen et al., 2018b). In this setting, the offset was attributed to the development of sulfidic porewaters (up to 1,500 μM) associated with the degradation of organic matter and the precipitation of authigenic U. As previously discussed, the microbial mats at Shark Bay are anoxic below 5 mm depth with sulfide concentrations of up to 250 μM. The lower sulfide concentrations at Shark Bay appears to result in less accumulation of authigenic U. For instance, the U concentrations in primary carbonate precipitates from the Bahamas were ~1.5 μg/g, which increased to ~4 μg/g in the carbonate core sediments, whereas the U concentrations in modern aragonitic crusts of stromatolites from Shark Bay ranged from 0.3 to 1.1 μg/g and U in older materials from SBS-1 and SBS-2 ranged from 0.6 to 1.8 μg/g. Thus, it appears that the net increase of authigenic U in carbonates from the Shark Bay is smaller than that in the Bahamas.

There appears to be an important role for organic matter remineralisation in controlling the local redox conditions in stromatolites at Shark Bay. This is indicated, for instance, in SBS-1 by the strong inverse correlation of $\delta^{238}U$ with TOC ($r = -0.91$; $n = 7$; $p = 0.03$) and a positive correlation with Mn contents ($r = 0.95$; $n = 7$; $p = 0.03$; Fig. 6), which support a mechanism whereby authigenic U is accumulated under reducing conditions (Fig. 6) associated with preferential reduction of ^{238}U. This is reasonable considering reducing conditions prevail within a few mm of the stromatolite surfaces at Shark Bay, resulting in large concentration gradients of O_2 and H_2S (Wong et al., 2015). Importantly, the relatively low TOC contents of stromatolites (<1 wt%) suggest that only a small amount of organic C must be remineralised to strongly modify $\delta^{238}U$. One implication of the heavily modified $\delta^{238}U$ in older stromatolite laminae is that the U system is unlikely to be 'closed' because this would result in quantitative U precipitation and no U isotope fractionation from seawater.

The $\delta^{238}U$ value (+0.11‰) of the stromatolite substrate at the base of SBS-1 is significantly higher than the stromatolite laminae and not related to modern stromatolite development in Shark Bay. This material has a minimum radiocarbon age of 14,850 ± 205 cal. years BP and is likely derived from older basement rocks, e.g., the Bibra Limestone of Late Pleistocene age, that were transported into shallow water (Chivas et al., 1990). In addition to the high degree of cementation relative to stromatolite laminae, clear evidence of a different origin for this substrate is provided by the lower $\delta^{13}C$ (−1.5‰) and TOC contents (Table 3), and higher Mn and Fe concentrations compared to SBS-1-A to -F (Table 4). These data support a component-selective approach where substrate materials should preferentially be avoided.

6.4. Considerations for reconstructing global redox conditions using ancient stromatolites

Accurately reconstructing seawater $\delta^{238}U$ using carbonates is essential for reconstructing seafloor anoxia using global U isotope mass balance models (e.g., Lau et al., 2016; Tostevin et al., 2019; Zhang et al., 2019; Kipp and Tissot, 2022b). Here we contextualise our results in terms of the two main approaches that might be useful for using stromatolitic carbonates as archives of seawater $\delta^{238}U$: (1) detailed petrographic investigations targeting specific components and (2) the application of a global offset factor to account for carbonate alteration effects.

A key finding of our study is that modern stromatolite crusts from the intertidal and subtidal zones preserve seawater-like $\delta^{238}U$ signatures. This contrasts with previous studies suggesting that the 'depositional components' of microbial carbonates, which form during the initial carbonate precipitation stage, yield a more variable $\delta^{238}U$ composition compared to marine (diagenetic) cements and were not reliable archives of seawater $\delta^{238}U$ (Hood et al., 2016). In fact, despite the large variability caused by post-depositional alteration processes, the average $\delta^{238}U$ of depositional micrites from dolomitic redbeds and peloidal grainstones, and dolomite and limestone microbial framework components (ca. −0.3‰) in Cryogenian marine carbonates analysed by Hood et al. (2016) are remarkably similar to the average value of modern aragonitic crusts of stromatolite from the intertidal and subtidal zones at Shark Bay (−0.32 ± 0.02, 1.s.d, n = 5; Fig. 7a). This may support a probabilistic approach for reconstructing the history of seawater $\delta^{238}U$ in ancient carbonates, requiring a detailed petrographic approach for single samples rather than integrating data from across large stratigraphic units. However, this approach should ideally be combined with a large sample dataset together with studies from multiple coeval sections.

In lieu of a detailed petrographic approach, a correction factor (or offset) can be applied to account for diagenetic effects (Romaniello et al., 2013; Chen et al., 2018a), but it remains to be confirmed if this is applicable to all settings; our results provide the first data for evaluating stromatolite records. Typically, a global offset of +0.27 ± 0.14‰ (1 s.d.) is applied to carbonate records to reconstruct seawater $\delta^{238}U$, which is derived from bulk carbonate sediments on the modern Bahamian platform (Romaniello et al., 2013; Chen et al., 2018b; Tissot et al., 2018). Key evidence supporting the reliability of this approach derives from the consistency in U isotope trends between coeval stratigraphic sections from different basins globally (e.g., Zhang et al., 2018; McDonald et al., 2022). However, this offset may vary across different depositional environments and even within the same locality. For instance, analyses of brachiopod shells and the bulk carbonate matrix from adjacent beds in Silurian limestones showed that a +0.3‰ offset was appropriate for some samples, but others displayed no offset from the inferred $\delta^{238}U$ value of Silurian seawater (del Rey et al., 2020), but a study of fossil brachiopod shells from the early to late Permian found that only ~50% of the shells preserved a primary, seawater-like $\delta^{238}U$ signature (Wang et al., 2022). Thus, some variations in carbonate $\delta^{238}U$ may reflect the variable degree of U(VI) exchange between reduced porewaters and seawater rather than global changes in redox state. At Shark Bay, stromatolite $\delta^{238}U$ values are offset from modern seawater by an average of +0.13 ± 0.11‰ (1 s.d.; Fig. 7B), which is on the lower end of the estimated offset from the Bahamas.

Key assumptions are required when applying a $\delta^{238}U$ offset to Precambrian carbonates based on data from modern shallow marine carbonates. One is that the ^{238}U-enrichment process only occurs in shallow sediments and does not operate at depth. This is largely supported by the near-zero U concentrations found in the porewaters of deep Bahamian drill cores (Site 1006), which also exhibit a closed-system behaviour for the ^{230}Th-^{234}U-^{238}U radioactive decay system (Henderson et al., 1999), and the narrow range of $\delta^{238}U$ values for the corresponding sediment horizons (Chen et al., 2018a). Thus, sediment porewaters can become closed to U isotope exchange with increasing depth and there are no subse-

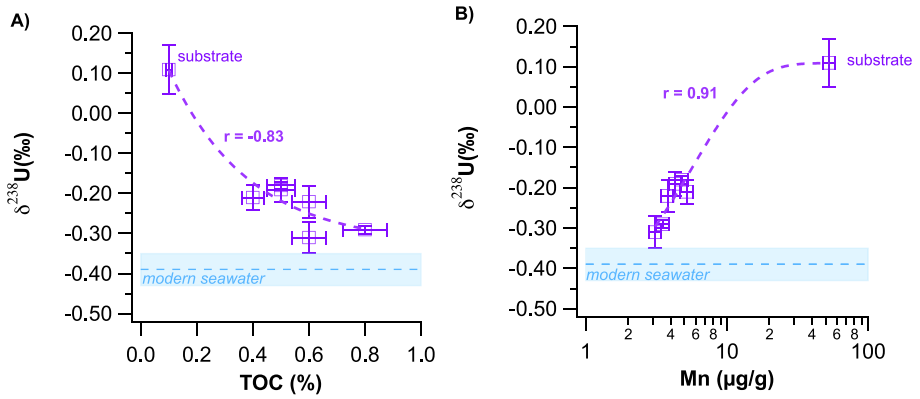

Fig. 6. Plots of $\delta^{238}U$ vs (A) TOC and (B) Mn contents in stromatolite SBS-1. The blue dashed line shows the average $\delta^{238}U$ value for modern seawater and the shaded blue area represents 1σ standard deviation around the mean (compiled data in Table S1). (For interpretation of the references to colour in this figure legend, the reader is referred to the web version of this article.)

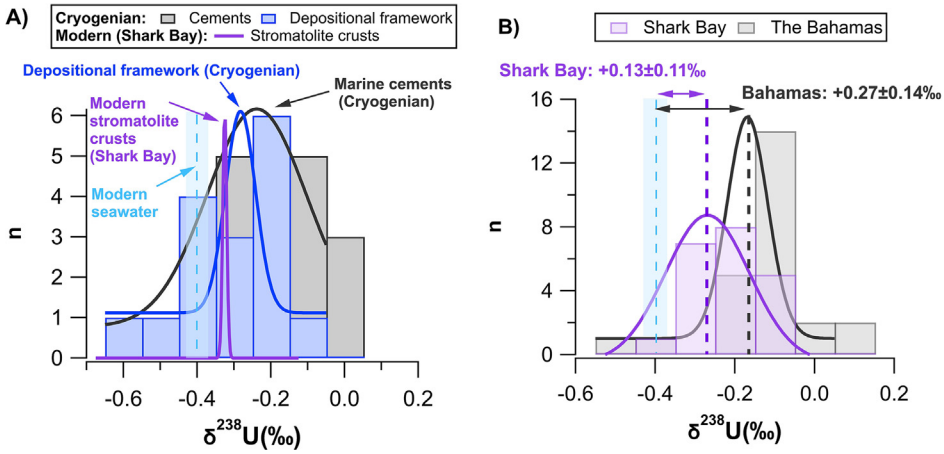

Fig. 7. Histograms and fitted Gaussian curves of $\delta^{238}U$ measurements in: (A) marine cements and depositional framework of Cryogenian marine carbonates (Hood et al., 2016), and modern stromatolite crusts from Shark Bay (histogram not shown due to narrow distribution); (B) sub-recent Shark Bay stromatolite laminae. The light blue dashed lines and shaded areas represent 1σ standard deviation around the mean for modern seawater (see compiled data in Table S1). (For interpretation of the references to colour in this figure legend, the reader is referred to the web version of this article.)

quent effects associated with burial diagenesis following the initial $\delta^{238}U$ offset of 0.2–0.4‰. This assumption might also apply to Precambrian carbonates, as it is likely that the U oceanic reservoir was much smaller than that of the modern oxic oceans and much less U would likely have been available to accumulate in carbonate sediments below a reduced/low-U water column. Thus, the expressed U isotope fractionation associated with this limited amount of authigenic U would be muted.

Another assumption is that carbonate sediment burial in modern settings from which the offsets are derived, e.g., the Bahamas, is representative for Precambrian carbonate sediments, which were mostly deposited in subsiding sedimentary basins on continental margins and experienced greater burial depths. Thus, the diminished U pore-fluid argument may not be valid for these Precambrian systems where subsurface fluids derived from meteoric waters may percolate through the basin and modify primary carbonate $\delta^{238}U$ signatures. As U is not generally considered a fluid-mobile element, a significant redistribution of U is not expected during burial and low-grade metamorphism. Moreover, metamorphic alterations effects can be minimised by limiting studies to rocks at the sub-greenschist facies, as is the case for other more-volatile isotopic systems, such as nitrogen (Bebout and Fogel, 1992). Finally, although our results provide insights into the potential modification of $\delta^{238}U$ during stromatolite formation, robustly interpreting Precambrian stromatolite records would benefit from systematic studies into sedimentary diagenesis associated with meteoric fluid flow in continental settings.

7. Conclusions

Our results show that modern stromatolite crusts from the subtidal and intertidal zones around Shark Bay record a near-primary U isotope signature of seawater and, thus, may be useful archives for reconstructing early Earth oceanic and atmospheric redox evolution and past changes in the areal expansion of seafloor anoxia. We investigated whether this effect is caused by involving U isotope fractionation effects between different dissolved U species found in aragonite co-precipitation experiments by Chen et al. (2016). This is because the restricted inflow of seawater into Shark Bay and the high evaporation rates at Shark Bay yield hypersaline seawater, which results in increased Ca concentrations and a higher proportion of dissolved U present as $Ca_2UO_2(CO_3)_3$. However, it appears that the $\delta^{238}U$ offset of ~0.05–0.07‰ from seawater for modern aragonitic crusts of stromatolites in Shark Bay cannot be explained by the higher proportion of neutral U species in Shark Bay seawater. Explaining this offset requires further inves-

tigation into the local chemistry at calcification sites during microbially mediated (or influenced) carbonate precipitation.

The seawater-like U isotope signature in modern aragonitic crusts of stromatolites from Shark Bay appears to be modified over relatively short timescales (<1 ka) in sub-recent stromatolite laminae. This results in an additional $\delta^{238}U$ offset of +0.13 ± 0.11‰ (1 s.d.) from seawater due to U addition under reducing conditions, likely associated with the remineralisation of organic material. A similar mechanism was proposed to explain a $\delta^{238}U$ offset from modern seawater for bulk carbonate sediments on the Bahamian platform (+0.27 ± 0.14‰; Romaniello et al., 2013; Chen et al., 2018a). As the offset derived from the Bahamian data is lower than – but within one standard deviation of – the offset based on the Shark Bay stromatolites data, our data provide important constraints for reconstructing past changes in seawater anoxia using $\delta^{238}U$ records from ancient carbonates, particularly stromatolitic limestones and dolostones. Alternatively, the seawater-like $\delta^{238}U$ signature of modern stromatolites suggest that targeting the primary depositional framework in ancient stromatolites, e.g., micritic laminae rather than late-stage marine cements, may be a viable approach for accurately reconstructing past changes in seawater $\delta^{238}U$.

Declaration of Competing Interest

The authors declare that they have no known competing financial interests or personal relationships that could have appeared to influence the work reported in this paper.

Acknowledgements

We would like to acknowledge the Malgana Peoples as the traditional custodians of the land and sea in and around the Shark Bay area, and pay our respects to their Elders past, present and emerging. We thank the Department of Biodiversity, Conservation and Attractions, Government of Western Australia for granting a permit to sample the stromatolites in Hamelin Pool, and Luke Skinner and Brad Lyons at Parks and Wildlife Service, Department of Biodiversity, Conservation and Attractions in Denham, Western Australia, for their invaluable advice and assistance with sampling. Dr. Ingo Horn is thanked for sharing his expertise during ICP-MS and MC-ICP-MS measurements and Dr. Hubert Vonhof is thanked for advising on sample analysis protocol and providing expertise for the stable isotope analyses. We also thank Xinming Chen and two anonymous reviewers for their constructive and valuable comments, as well as Claudine Stirling for her valuable advice and editorial handling of the manuscript. Funding for ANM was provided by the Deutsche Forschungsgemeinschaft (DFG) priority program 'SPP-1833 Building a Habitable Earth'.

Appendix A. Supplementary material

The supplementary document associated with this paper contains data tables, correlation matrices and X-ray diffraction spectra for the material analysed in this study. The raw X-ray diffraction data are provided as a separate .csv file. Supplementary material to this article can be found online at https://doi.org/10.1016/j.gca.2023.01.011.

References

Abe, M., Suzuki, T., Fujii, Y., Hada, M., Hirao, K., 2008. An ab initio molecular orbital study of the nuclear volume effects in uranium isotope fractionations. J. Chem. Phys. 129, 1–7.

Albut, G., Kamber, B.S., Brüske, A., Beukes, N.J., Smith, A.J.B., Schoenberg, R., 2019. Modern weathering in outcrop samples versus ancient paleoredox information in drill core samples from a Mesoarchaean marine oxygen oasis in Pongola Supergroup, South Africa. *Geochim. Cosmochim. Acta* 265, 330–353.

Allwood, A.C., Walter, M.R., Kamber, B.S., Marshall, C.P., Burch, I.W., 2006. Stromatolite reef from the Early Archaean era of Australia. Nature 441, 714–718.

Andersen, M.B., Romaniello, S., Vance, D., Little, S.H., Herdman, R., Lyons, T.W., 2014. A modern framework for the interpretation of $^{238}U/^{235}U$ in studies of ancient ocean redox. Earth Planet. Sci. Lett. 400, 184–194.

Andersen, M.B., Stirling, C.H., Weyer, S., 2017. Uranium Isotope Fractionation. Rev. Miner. Geochem. 82, 799–850.

Asael, D., Tissot, F.L.H., Reinhard, C.T., Rouxel, O., Dauphas, N., Lyons, T.W., Ponzevera, E., Liorzou, C., Chéron, S., 2013. Coupled molybdenum, iron and uranium stable isotopes as oceanic paleoredox proxies during the Paleoproterozoic Shunga Event. Chem. Geol. 362, 193–210.

Bebout, G.E., Fogel, M.L., 1992. Nitrogen-isotope compositions of metasedimentary rocks in the Catalina Schist, California: Implications for metamorphic devolatilization history. Geochim. Cosmochim. Acta 56, 2839–2849.

Bekker, A., Holland, H.D., Wang, P.L., Rumble, D., Stein, H.J., Hannah, J.L., Coetzee, L.L., Beukes, N.J., 2004. Dating the rise of atmospheric oxygen. Nature 427, 117–120.

Bigeleisen, J., 1996. Nuclear size and shape effects in chemical reactions. Isotope chemistry of the heavy elements. J. Am. Chem. Soc. 118, 3676–3680.

Bolhar, R., Hofmann, A., Woodhead, J., Hergt, J., Dirks, P., 2002. Pb- and Nd-isotope systematics of stromatolitic limestones from the 2.7 Ga Ngezi group of the Belingwe Greenstone Belt: Constraints on timing of deposition and provenance. Precambrian Res. 114, 277–294.

Bolhar, R., Hofmann, A., Siahi, M., Feng, Y.X., Delvigne, C., 2015. A trace element and Pb isotopic investigation into the provenance and deposition of stromatolitic carbonates, ironstones and associated shales of the ~3.0 Ga Pongola Supergroup, Kaapvaal Craton. *Geochim. Cosmochim. Acta* 158, 57–78.

Brady, A.L., Slater, G.F., Omelon, C.R., Southam, G., Druschel, G., Andersen, D.T., Hawes, I., Laval, B., Lim, D.S.S., 2010. Photosynthetic isotope biosignatures in laminated micro-stromatolitic and non-laminated nodules associated with modern, freshwater microbialites in Pavilion Lake, B.C. Chem. Geol. 274, 56–67.

Brennecka, G.A., Herrmann, A.D., Algeo, T.J., Anbar, A.D., 2011. Rapid expansion of oceanic anoxia immediately before the end-Permian mass extinction. Proc. Natl. Acad. Sci. U. S. A. 108, 17631–17634.

Bryan, E., Meredith, K.T., Baker, A., Post, V.E.A., Andersen, M.S., 2016. Island groundwater resources, impacts of abstraction and a drying climate: Rottnest Island, Western Australia. J. Hydrol. 542, 704–718.

Brüske, A., Martin, A.N., Rammensee, P., Eroglu, S., Lazarov, M., Albut, G., Schuth, S., Aulbach, S., Schoenberg, R., Beukes, N., Hofmann, A., Nägler, T., Weyer, S., 2020a. The onset of oxidative weathering traced by uranium isotopes. Precambrian Res. 338, 1–16.

Brüske, A., Weyer, S., Zhao, M.-Y., Planavsky, N.J., Wegwerth, A., Neubert, N., Dellwig, O., Lau, K.V., Lyons, T.W., 2020b. Correlated molybdenum and uranium isotope signatures in modern anoxic sediments: implications for their use as paleo-redox proxy. Geochim. Cosmochim. Acta 270, 449–474.

Chen, X., Romaniello, S.J., Herrmann, A.D., Wasylenki, L.E., Anbar, A.D., 2016. Uranium isotope fractionation during coprecipitation with aragonite and calcite. Geochim. Cosmochim. Acta 188, 189–207.

Chen, X., Romaniello, S.J., Anbar, A.D., 2017. Uranium isotope fractionation induced by aqueous speciation: Implications for U isotopes in marine $CaCO_3$ as a paleoredox proxy. Geochim. Cosmochim. Acta 215, 162–172.

Chen, X., Romaniello, S.J., Herrmann, A.D., Hardisty, D., Gill, B.C., Anbar, A.D., 2018a. Diagenetic effects on uranium isotope fractionation in carbonate sediments from the Bahamas. Geochim. Cosmochim. Acta 237, 294–311.

Chen, X., Romaniello, S.J., Herrmann, A.D., Samankassou, E., Anbar, A.D., 2018b. Biological effects on uranium isotope fractionation ($^{238}U/^{235}U$) in primary biogenic carbonates. Geochim. Cosmochim. Acta 240, 1–10.

Chen, X., Tissot, F.L.H., Jansen, M.F., Bekker, A., Liu, C.X., Nie, N.X., Halverson, G.P., Veizer, J., Dauphas, N., 2021. The uranium isotopic record of shales and carbonates through geologic time. Geochim. Cosmochim. Acta 300, 164–191.

Chen, X., 2020. Aqueous uranium speciation on U/Ca in foraminiferal calcite: The importance of minor species - $UO_2(CO_3)_2^2$. ACS Earth Sp. Chem. 4, 2050–2060.

Cheng, H., Edwards, R.L., Hoff, J., Gallup, C.D., Richards, D.A., Asmerom, Y., 2000. The half-lives of uranium-234 and thorium-230. Chem. Geol. 169, 17–33.

Chivas, A.R., Torgersen, T., Polach, H.A., 1990. Growth rates and Holocene development of stromatolites from Shark Bay, Western Australia. *Aust. J. Earth Sci.* 37, 113–121.

Clarkson, M.O., Stirling, C.H., Jenkyns, H.C., Dickson, A.J., Porcelli, D., Moy, C.M., Pogge von Strandmann, P.A.E., Cooke, I.R., Lenton, T.M., 2018. Uranium isotope evidence for two episodes of deoxygenation during Oceanic Anoxic Event 2. Proc. Natl. Acad. Sci. U. S. A. 115, 2918–2923.

Clarkson, M.O., Müsing, K., Andersen, M.B., Vance, D., 2020. Examining pelagic carbonate-rich sediments as an archive for authigenic uranium and molybdenum isotopes using reductive cleaning and leaching experiments. Chem. Geol. 539, 119412.

Clarkson, M.O., Lenton, T.M., Andersen, M.B., Bagard, M.L., Dickson, A.J., Vance, D., 2021. Upper limits on the extent of seafloor anoxia during the PETM from uranium isotopes. Nat. Commun. 12, 1–9.

Dahl, T.W., Boyle, R.A., Canfield, D.E., Connelly, J.N., Gill, B.C., Lenton, T.M., Bizzarro, M., 2014. Uranium isotopes distinguish two geochemically distinct stages during the later Cambrian SPICE event. Earth Planet. Sci. Lett. 401, 313–326.

De Graaf, S., Vonhof, H.B., Levy, E.J., Markowska, M., Haug, G.H., 2021. Isotope ratio infrared spectroscopy analysis of water samples without memory effects. Rapid Commun. Mass Spectrom. 35, e9055.

del Rey, Á., Havsteen, J.C., Bizzarro, M., Dahl, T.W., 2020. Untangling the diagenetic history of uranium isotopes in marine carbonates: A case study tracing the $\delta^{238}U$ composition of late Silurian oceans using calcitic brachiopod shells. Geochim. Cosmochim. Acta 287, 93–110.

Dong, W., Brooks, S.C., 2006. Determination of the formation constants of ternary complexes of uranyl and carbonate with alkaline earth metals (Mg^{2+}, Ca^{2+}, Sr^{2+}, and Ba^{2+}) using anion exchange method. Environ. sci. tech. 40 (15), 4689–4695.

Dravis, J.J., 1982. Hardened subtidal stromatolites, Bahamas. Science 219, 385–386.

Dupraz, C., Reid, R.P., Braissant, O., Decho, A.W., Norman, R.S., Visscher, P.T., 2009. Processes of carbonate precipitation in modern microbial mats. Earth-Sci. Rev. 96, 141–162.

Elrick, M., Polyak, V., Algeo, T.J., Romaniello, S., Asmerom, Y., Herrmann, A.D., Anbar, A.D., Zhao, L., Chen, Z.Q., 2017. Global-ocean redox variation during the middle-late Permian through Early Triassic based on uranium isotope and Th/U trends of marine carbonates. Geology 45, 163–166.

Endrizzi, F., Leggett, C.J., Rao, L., 2016. Scientific basis for efficient extraction of uranium from seawater. I: Understanding the chemical speciation of uranium under seawater conditions. Ind. Eng. Chem. Res. 55, 4249–4256.

Farquhar, J., Bao, H., Thiemens, M., 2000. Atmospheric influence of Earth's earliest sulfur cycle. Science 289, 756–758.

Fujii, T., Moynier, F., Albarède, F., 2009. The nuclear field shift effect in chemical exchange reactions. Chem. Geol. 267, 139–156.

Geyman, E.C., Maloof, A.C., 2019. A diurnal carbon engine explains 13C-enriched carbonates without increasing the global production of oxygen. Proc. Nation. Acad. Sci. 116 (49), 24433–24439.

Gilleaudeau, G.J., Romaniello, S.J., Luo, G., Kaufman, A.J., Zhang, F., Klaebe, R.M., Kah, L.C., Azmy, K., Bartley, J.K., Zheng, W., Knoll, A.H., Anbar, A.D., 2019. Uranium isotope evidence for limited euxinia in mid-Proterozoic oceans. Earth Planet. Sci. Lett. 521, 150–157.

Goto, K.T., Anbar, A.D., Gordon, G.W., Romaniello, S.J., Shimoda, G., Takaya, Y., Tokumaru, A., Nozaki, T., Suzuki, K., Machida, S., Hanyu, T., Usui, A., 2014. Uranium isotope systematics of ferromanganese crusts in the Pacific Ocean: Implications for the marine $^{238}U/^{235}U$ isotope system. Geochim. Cosmochim. Acta 146, 43–58.

Grenthe, I., Fuger, J., Konings, R.J., Lemire, R.J., Muller, A.B., Nguyen-Trung, C., Wanner, H., 1992. Chemical thermodynamics of uranium, 1. Elsevier, Amsterdam.

Grotzinger, J.P., 1990. Geochemical model for Proterozoic stromatolite decline. Am. J. Sci. 290, 80–103.

Henderson, G.M., Slowey, N.C., Haddad, G.A., 1999. Fluid flow through carbonate platforms: Constraints from $^{234}U/^{238}U$ and Cl^- in Bahamas pore-waters. Earth Planet. Sci. Lett. 169, 99–111.

Holland, H.D., 2002. Volcanic gases, black smokers, and the Great Oxidation Event. Geochim. Cosmochim. Acta 66, 3811–3826.

Hood, A.V.S., Planavsky, N.J., Wallace, M.W., Wang, X., Bellefroid, E.J., Gueguen, B., Cole, D.B., 2016. Integrated geochemical-petrographic insights from componentselective $\delta^{238}U$ of Cryogenian marine carbonates. Geology 44, 935–938.

Jahnert, R.J., Collins, L.B., 2012. Characteristics, distribution and morphogenesis of subtidal microbial systems in Shark Bay, Australia. *Mar. Geol.* 303, 115–136.

Jost, A.B., Bachan, A., van de Schootbrugge, B., Lau, K.V., Weaver, K.L., Maher, K., Payne, J.L., 2017. Uranium isotope evidence for an expansion of marine anoxia during the end-Triassic extinction. Geochem. Geophys. Geosyst. 18, 3093–3108.

Kipp, M.A., Tissot, F.L., 2022b. Inverse methods for consistent quantification of seafloor anoxia using uranium isotope data from marine sediments. Earth and Planetary Science Letters 577, 117240.

Kipp, M.A., Li, H., Ellwood, M.J., John, S.G., Middag, R., Adkins, J.F., Tissot, F.L., 2022a. ^{238}U, ^{235}U and ^{234}U in seawater and deep-sea corals: A high-precision reappraisal. Geochimica et Cosmochimica Acta 336, 231–248.

Lau, K.V., Maher, K., Altiner, D., Kelley, B.M., Kump, L.R., Lehrmann, D.J., Silva-Tamayo, J.C., Weaver, K.L., Yu, M., Payne, J.L., 2016. Marine anoxia and delayed Earth system recovery after the end-Permian extinction. Proc. Natl. Acad. Sci. U. S. A. 113, 2360–2365.

Lau, K.V., Macdonald, F.A., Maher, K., Payne, J.L., 2017. Uranium isotope evidence for temporary ocean oxygenation in the aftermath of the Sturtian Snowball Earth. Earth Planet. Sci. Lett. 458, 282–292.

Livermore, B.D., Dahl, T.W., Bizzarro, M., Connelly, J.N., 2020. Uranium isotope compositions of biogenic carbonates – Implications for U uptake in shells and the application of the paleo-ocean oxygenation proxy. Geochim. Cosmochim. Acta 287, 50–64.

Logan, B.W., 1961. Cryptozoon and associate stromatolites from the Recent, Shark Bay, Western Australia. J. Geol. 69, 517–533.

McDonald, B.S., Partin, C.A., Sageman, B., Holmden, C., 2022. Uranium isotope reconstruction of ocean deoxygenation during OAE 2 hampered by uncertainties in fractionation factors and local U-cycling. Geochim. Cosmochim. Acta 331, 143–164.

Morris, T.E., Visscher, P.T., O'Leary, M.J., Fearns, P.R.C.S., Collins, L.B., 2020. The biogeomorphology of Shark Bay's microbialite coasts. Earth-Sci. Rev. 205, 102921.

Murphy, M.J., Stirling, C.H., Kaltenbach, A., Turner, S.P., Schaefer, B.F., 2014. Fractionation of $^{238}U/^{235}U$ by reduction during low temperature uranium mineralisation processes. Earth Planet. Sci. Lett. 388, 306–317.

Noordmann, J., Weyer, S., Montoya-Pino, C., Dellwig, O., Neubert, N., Eckert, S., Paetzel, M., Böttcher, M.E., 2015. Uranium and molybdenum isotope systematics in modern euxinic basins: Case studies from the central Baltic Sea and the Kyllaren fjord (Norway). Chem. Geol. 396, 182–195.

Nutman, A.P., Bennett, V.C., Friend, C.R.L.L., Van Kranendonk, M.J., Chivas, A.R., 2016. Rapid emergence of life shown by discovery of 3,700-million-year-old microbial structures. Nature 537, 535–538.

Parkhurst, D.L., Appelo, C.A.J., 2013. Description of input and examples for PHREEQC version 3—a computer program for speciation, batch-reaction, one-dimensional transport, and inverse geochemical calculations. US Geol. Surv. Tech. Methods 6, 497.

Peters, S.E., Husson, J.M., Wilcots, J., 2017. The rise and fall of stromatolites in shallow marine environments. Geology 45, 487–490.

Plater, A.J., Ivanovich, M., Dugdale, R.E., 1992. Uranium series disequilibrium in river sediments and waters: the significance of anomalous activity ratios. Appl. Geochem. 7, 101–110.

Playford, P.E., Cockbain, A.E., 1976. Modern Algal Stromatolites at Hamelin Pool, A Hypersaline Barred Basin in Shark Bay, Western Australia. Dev. Sedimentol. 20, 389–411.

Reid, R.P., James, N.P., Macintyre, I.G., Dupraz, C.P., Burne, R.V., 2003. Shark Bay stromatolites: Microfabrics and reinterpretation of origins. Facies 20, 299–324.

Richter, S., Alonso, A., Bolle, W., De, K.H., Verbruggen, A., Wellum, R., Taylor, P.D.P., 2005. Re-certification of a series of uranium isotope reference materials: IRMM-183, IRMM-184, IRMM-185, IRMM-186 and IRMM-187. Int. J. Mass Spectrom. 247, 37–39.

Richter, S., Alonso-Munoz, A., Eykens, R., Jacobsson, U., Kuehn, H., Verbruggen, A., Aregbe, Y., Wellum, R., Keegan, E., 2008. The isotopic composition of natural uranium samples-Measurements using the new $n(^{233}U)/n(^{236}U)$ double spike IRMM-3636. Int. J. Mass Spectrom. 269, 145–148.

Richter, S., Eykens, R., Kühn, H., Aregbe, Y., Verbruggen, A., Weyer, S., 2010. New average values for the $n(^{238}U)/n(^{235}U)$ isotope ratios of natural uranium standards. Int. J. Mass Spectrom. 295, 94–97.

Riding, R., 2011. Microbialites, stromatolites, and thrombolites. Encycl. Earth Sci. Ser., 635–654

Romaniello, S.J., Herrmann, A.D., Anbar, A.D., 2013. Uranium concentrations and $^{238}U/^{235}U$ isotope ratios in modern carbonates from the Bahamas: Assessing a novel paleoredox proxy. Chem. Geol. 362, 305–316.

Schauble, E.A., 2007. Role of nuclear volume in driving equilibrium stable isotope fractionation of mercury, thallium, and other very heavy elements. Geochim. Cosmochim. Acta 71, 2170–2189.

Stirling, C.H., Andersen, M.B., Potter, E.-K., Halliday, A.N., 2007. Low-temperature isotopic fractionation of uranium. Earth Planet. Sci. Lett. 264, 208–225.

Suosaari, E.P., Reid, R.P., Playford, P.E., Foster, J.S., Stolz, J.F., Casaburi, G., Hagan, P.D., Chirayath, V., Macintyre, I.G., Planavsky, N.J., 2016. New multi-scale perspectives on the stromatolites of Shark Bay, Western Australia. Sci. Rep. 6, 1–13.

Tissot, F.L.H., Dauphas, N., 2015. Uranium isotopic compositions of the crust and ocean: Age corrections, U budget and global extent of modern anoxia. Geochim. Cosmochim. Acta 167, 113–143.

Tissot, F.L.H., Chen, C., Go, B.M., Naziemiec, M., Healy, G., Bekker, A., Swart, P.K., Dauphas, N., 2018. Controls of eustasy and diagenesis on the $^{238}U/^{235}U$ of carbonates and evolution of the seawater ($^{234}U/^{238}U$) during the last 1.4 Myr. Geochim. Cosmochim. Acta 242, 233–265.

Tostevin, R., Clarkson, M.O., Gangl, S., Shields, G.A., Wood, R.A., Bowyer, F., Penny, A. M., Stirling, C.H., 2019. Uranium isotope evidence for an expansion of anoxia in terminal Ediacaran oceans. Earth Planet. Sci. Lett. 506, 104–112.

Walter, M.R., Heys, G.R., 1985. Links between the rise of the metazoa and the decline of stromatolites. Precambrian Res. 29, 149–174.

Wang, X., Planavsky, N.J., Hofmann, A., Saupe, E.E., De Corte, B.P., Philippot, P., LaLonde, S.V., Jemison, N.E., Zou, H., Ossa, F.O., Rybacki, K., Alfimova, N., Larson, M.J., Tsikos, H., Fralick, P.W., Johnson, T.M., Knudsen, A.C., Reinhard, C.T., Konhauser, K.O., 2018. A Mesoarchean shift in uranium isotope systematics. Geochim. Cosmochim. Acta 238, 438–452.

Wang, W., Zhang, F., Shen, S., Bizzarro, M., Garbelli, C., Zheng, Q., Zhang, Y., Yuan, D., Shi, Y., Cao, M., Dahl, T.W., 2022. Constraining marine anoxia under the extremely oxygenated Permian atmosphere using uranium isotopes in calcitic brachiopods and marine carbonates. Earth Planet. Sci. Lett. 594, 117714.

Weyer, S., Anbar, A.D., Gerdes, A., Gordon, G.W., Algeo, T.J., Boyle, E.A., 2008. Natural fractionation of $^{238}U/^{235}U$. Geochim. Cosmochim. Acta 72, 345–359.

Wong, H.L., Smith, D.-L., Visscher, P.T., Burns, B.P., 2015. Niche differentiation of bacterial communities at a millimeter scale in Shark Bay microbial mats. Sci. Rep. 5, 15607.

Zhang, F., Algeo, T.J., Romaniello, S.J., Cui, Y., Zhao, L., Chen, Z.Q., Anbar, A.D., 2018. Congruent Permian-Triassic $\delta^{238}U$ records at Panthalassic and Tethyan sites: Confirmation of global-oceanic anoxia and validation of the U-isotope paleoredox proxy. Geology 46, 327–330.

Zhang, F., Xiao, S., Romaniello, S.J., Hardisty, D., Li, C., Melezhik, V., Pokrovsky, B., Cheng, M., Shi, W., Lenton, T.M., Anbar, A.D., 2019. Global marine redox changes drove the rise and fall of the Ediacara biota. Geobiology 17, 594–610.

Zhang, F., Lenton, T.M., del Rey, Á., Romaniello, S.J., Chen, X., Planavsky, N.J., Clarkson, M.O., Dahl, T.W., Lau, K.V., Wang, W., Li, Z., Zhao, M., Isson, T., Algeo, T. J., Anbar, A.D., 2020. Uranium isotopes in marine carbonates as a global ocean paleoredox proxy: A critical review. Geochim. Cosmochim. Acta 287 (287), 27–49.